International Journal of Concrete Structures and Materials

RESEARCH Open Access

Alkali Silica Reactivity in Cement Composite with Ferronickel Slag Aggregates: A Regression Analysis and 3D Visualisation Approach

Tae Yeon Kim[1], Sun Gyu Park[2], Woo Jin Lee[3], Jae Hun Jung[1], Jun Chul Yoon[1], Kadepalli Nagendra Shivaprasad[4*] and Hyun Min Yang[5*]

Abstract

The utilisation of industrial by-products and waste materials as supplementary materials in cement-based composites offers a sustainable approach towards reducing environmental impact and optimising resource utilisation in construction. This study investigates the potential use of ferronickel slag (FNS) aggregates in cement mortar, focusing on their influence on alkali silica reactivity (ASR) and mechanical properties. The compressive strength of mortar mixes was evaluated at different water to cement ratio, with varying proportions of FNS as a replacement for natural sand. The results revealed that a 50% replacement of standard sand with FNS aggregates yielded the highest compressive strength, reaching a maximum of 59.49 MPa. Full replacement with FNS aggregates ASR expansion tests indicated that FNS aggregates are highly reactive in NaOH solutions, with expansion levels exceeding ASTM limits. However, innocuous expansion was observed in water and $Ca(OH)_2$ environments, highlighting their stabilizing effect. Regression analysis showed that use of FNS aggregates present challenges in strongly alkaline environments, they hold significant potential for enhancing the mechanical properties of cement mortar, particularly when used in balanced proportions.

Keywords Ferronickel slag waste, Cement mortar, Compressive strength, Alkali silica reaction, Regression analysis, 3D plots

1 Introduction

The escalating production of waste by industrial sectors poses a significant threat to the environment. Across the globe, numerous industries, including steel, aluminium, copper, zinc, and coal production, generate significant amounts of waste. The challenge lies in recognising and maximising the potential utilization of these waste materials as valuable byproducts (Kurniati et al., 2023; Saha et al., 2018; C. Shi & Qian, 2000). Importantly, many applications nowadays effectively utilise these industrial byproducts. Among them is FNS waste, a byproduct of smelting nickel ores to produce ferronickel alloys. The processing of nickel ore can result in the generation of slag ranging from 50 to 75% of the original material (Bartzas & Komnitsas, 2015; Tangahu et al., 2015). It has been estimated that for every ton of

Journal information: ISSN 1976-0485 / eISSN 2234-1315.

*Correspondence:
Kadepalli Nagendra Shivaprasad
shivaprasad.god@gmail.com
Hyun Min Yang
yhm04@hanyang.ac.kr
[1] Department of Smart City Engineering, Hanyang University, Sangnok-Gu, Ansan-Si 15588, Republic of Korea
[2] Department of Architectural Engineering, Mokwon University, Seo-Gu, Daejeon 35349, Republic of Korea
[3] Engineering Center, Samsung C&T, Gangdong-Gu, Seoul 05288, Republic of Korea
[4] Centre for AI Technology in Construction, Hanyang University, Sangnok-Gu, Ansan-Si 15588, Republic of Korea
[5] Division of Smart Convergence Engineering, Hanyang University, Sangnok-Gu, Ansan-Si 15588, Republic of Korea

nickel produced, approximately 14 tons of slag are generated (Jianwei Sun et al., 2019). In South Korea alone, more than two million tonnes of ferro nickel slag waste are produced annually (Cho et al., 2018). In general, FNS can be used as a substitute material for soil stabilization, asphalt pavements, mineral wool production, abrasives, and serpentine. Utilizing it in the construction industry as fine aggregates is an optimal solution.

Several studies have explored the utilization of blast furnace slag, a by-product of the steel industry, as a substitute material for cementitious materials (Jianwei Sun et al., 2018; Tang et al., 2022). Likewise, research has been conducted on the utilization of copper slag and zinc slag, byproducts of the copper and zinc industries, respectively. Similarly, after FNS cooling and crushing, these slag grains are mostly angular in shape and have low water absorption, high strength and high deformation resistance (Dong et al., 2021; Saha et al., 2018; Jianwei Sun et al., 2019; T. Yang et al., 2020). Sun et al. (Jianwei Sun et al., 2019) investigated the utilisation of two types of ferronickel industry slag, namely, electric furnace slag (ES) and blast furnace slag (BS), and demonstrated that FNS waste can be effectively utilised in cementitious systems as sand replacement. The results suggest that using 75% BS or 25% ES is the optimal choice for engineering applications. Similarly, the utilisation of FNS waste as a replacement for up to 50% of sand has shown a more than 10% increase in compressive strength compared to normal fine aggregate mixes (Saha & Sarker, 2017a; Saha et al., 2018; Togawa et al., 1996). Furthermore, various studies have investigated the application of FNS in concrete production and showed that the replacement of FNS for natural aggregates enhanced the compressive strength, workability, and carbonation resistance of the mortars and concrete (Akiyama & Yamamoto, 1986; Bao et al., 2021; Han et al., 2023; Irmawaty et al., 2023; Kurniati et al., 2023; Liu et al., 2020; Małek et al., 2021; Manso et al., 2006; Ngii et al., 2021; Nguyen et al., 2021; Nuruzzaman et al., 2022; Petrounias et al., 2022; Saha et al., 2018, 2019; Saha & Sarker, 2018; Jianwei Sun et al., 2019; Tang et al., 2022).

FNS consists mainly of SiO_2, MgO, and FeO, and traces of CaO, SO_3, K_2O etc. It is composed of non-crystalline minerals as well as a mixture of crystalline minerals, such as enstatite, forsterite, Olivine and diopside (Choi & Choi, 2015; Han et al., 2023). The chemical composition and characteristics of these crystalline and non-crystalline minerals vary with the production process (Choi & Choi, 2015; Jianwei Sun et al., 2019). Irrespective of the production process amorphous silica content presence in FNS aggregates is observed. This amorphous silica will undergo an ASR, which leads to a reduction in the durability of materials (Fernandes & Broekmans, 2013; Figueira et al., 2019; Olajide et al., 2023).

Various studies highlight the role of various factors such as compressive strength, aggregate content, and w/cm ratio as crucial in understanding the ASR behaviour in cementitious systems (Glinicki et al., 2023; Miura et al., 2022; Junbo Sun et al., 2021; Zhang et al., 2024). Including reactive aggregates, like FNS, which has shown potential for ASR expansion, further complicates the interaction. In recent years, growing interest has directed the researchers to use various models and techniques, including machine learning, to study the behaviour of reactive aggregates in cementitious systems (Aslani et al., 2023; Bulteel et al., 2002; Guthrie & Carey, 2015; Haha et al., 2007; Kumar Parhi & Kumar Panigrahi, 2024; Poyet et al. 2007.; Junbo Sun et al., 2021; Wang et al., 2023; L. Yang et al., 2023; Yu et al., 2020, 2019.; Zhang et al., 2024). Sun et al. (Junbo Sun et al., 2021) developed a beetle antennae search optimised random forest (BAS-RF) model to predict ASR expansion in waste glass cementitious composites, achieving a high correlation coefficient of 0.942 on the test set, which demonstrated superior accuracy compared to multiple linear and logistic regression models. The model was trained with data of ASR expansion samples with input features, including curing time, waste glass powder particle size, replacement ratio, and chemical activator content. Sensitivity analysis revealed that the WGP replacement ratio was the most significant factor affecting ASR expansion after curing time, confirming the experimental observations of ASR behaviour in these composites. Yang et al. (L. Yang et al., 2023) developed a hybrid artificial neural network (ANN) model, optimised using a beta differential evolution-improved particle swarm optimisation algorithm, to predict ASR expansion in concrete. Using a comprehensive database of ASR expansion data sets, the ANN model achieved high predictive accuracy, with coefficients of determination of 0.981 for training and 0.971 for testing, demonstrating its effectiveness in capturing the complex, nonlinear relationships governing ASR expansion. The model successfully reproduced experimental trends related to material composition, environmental conditions, specimen geometry, and time dependent behaviour, validating its robustness for ASR expansion prediction. Aslani et al. (Aslani et al., 2023) developed two back propagation neural network (BPNN) models such as LM-BPNN (Levenberg–Marquardt optimized) and BR-BPNN (Bayesian regularized) to predict ASR expansion in concrete, achieving test set R values of 0.926 and R = 0.912, respectively, using a database with inputs, including w/cm, alkali content, reactive aggregate ratios, temperature, and humidity. Sensitivity analysis revealed reactive aggregates content as the most critical

factor influencing ASR expansion, followed by alkali content and relative humidity, while non-reactive aggregates and temperature had minimal impact. The study highlighted the LM-BPNN's superior stability compared to BR-BPNN, providing a robust framework for ASR prediction in concrete mix optimisation. These predictive tools offer an efficient means to assess the durability of cement composites without relying solely on time intensive experimental testing.

Despite the growing use of predictive models in ASR research, limited studies that have focused specifically on FNS as a fine aggregate in cementitious systems. The main concerns regarding its alkali silica reactivity have hindered its widespread adoption in various applications. Furthermore, most ASR prediction models either do not incorporate industrial byproducts such as FNS or fail to visualise parameter interactions in an interpretable manner. This study addresses these gaps by experimentally evaluating ASR expansion in FNS containing mortars under various curing conditions, and developing a regression-based predictive model. The incorporation of 3D surface plots enhances understanding of the complex interdependencies among compressive strength, w/cm, and FNS content. The insights gained support both material selection and mix design optimisation for sustainable construction. Thus, the study not only contributes to the safe use of FNS in cementitious composites but also demonstrates the utility of visual, data driven modelling in durability assessment. To support this, a comprehensive testing program was conducted using mortar mixes with varying FNS replacement levels and w/cm, allowing evaluation across a wide performance spectrum.

1.1 Significance of the Study

The rapidly increasing demand for ferro nickel in critical sectors such as stainless steel and electronics has spurred industrial expansion, fostering economic prosperity worldwide. However, the production of ferro nickel presents inherent health risks to workers and local communities due to emissions of hazardous substances. While governmental bodies endeavour to address these health hazards, the disposal of the resulting waste remains a pressing concern. This study aims to provide a sustainable solution by exploring the potential use of FNS as a partial replacement for sand in cementitious composites. The integration of FNS in cement mortar not only addresses waste management concerns by diverting industrial by-products from landfills but also enhances the sustainability of construction practices by reducing the consumption of natural resources and energy-intensive materials.

Through regression analysis and 3D visualisation, this study investigates the influence of key variables, such as compressive strength, w/cm and FNS aggregate content on ASR in cement composites. The developed predictive models and 3D plots offer valuable insights into the optimal mix proportions for mitigating ASR expansion while enhancing material performance. This research provides a data driven approach to the repurposing of FNS in cementitious composites, offering a pathway for minimising environmental impacts while improving the durability and structural integrity of construction materials. Ultimately, the study promotes a safer, healthier environment and contributes to sustainable construction practices.

Table 1 Physical characteristics of the materials

Parameter	Standard sand	FNS
Specific gravity	2.60	2.81
Water absorption (%)	1.13	2.60
Fineness modulus	2.6	3.8
Percentage passing 75 µm sieve (%)	Nil	0.8

Table 2 Chemical composition of the materials

Material	Percentage Mass	
	Cement	FNS
CaO	67.83	1.18
SiO_2	18.05	49.95
Al_2O_3	3.96	2.03
Fe_2O_3	3.75	15.19
SO_3	3.52	0.12
MgO	1.62	31.49
K_2O	1.05	0.04
Na_2O	0.08	–

2 Materials

FNS was sourced locally for this study, while standard sand and ordinary Portland cement were used as the primary materials. The physical characteristics of the materials are presented in Table 1, while Table 2 presents the chemical compositions of the materials used in the study. Figure 1 presents images of fine aggregates both natural sand and FNS aggregates, illustrating a distinct difference in particle shapes. Natural sand exhibits a completely angular nature, characterised by sharp edges and corners. In contrast, the FNS aggregates comprise a diverse mix of both spherical and angular-shaped particles. Furthermore, Fig. 1 presents the XRD pattern of FNS, showing both crystalline and amorphous phases. The broad hump observed between 20 ° and 35 ° 2θ is characteristic

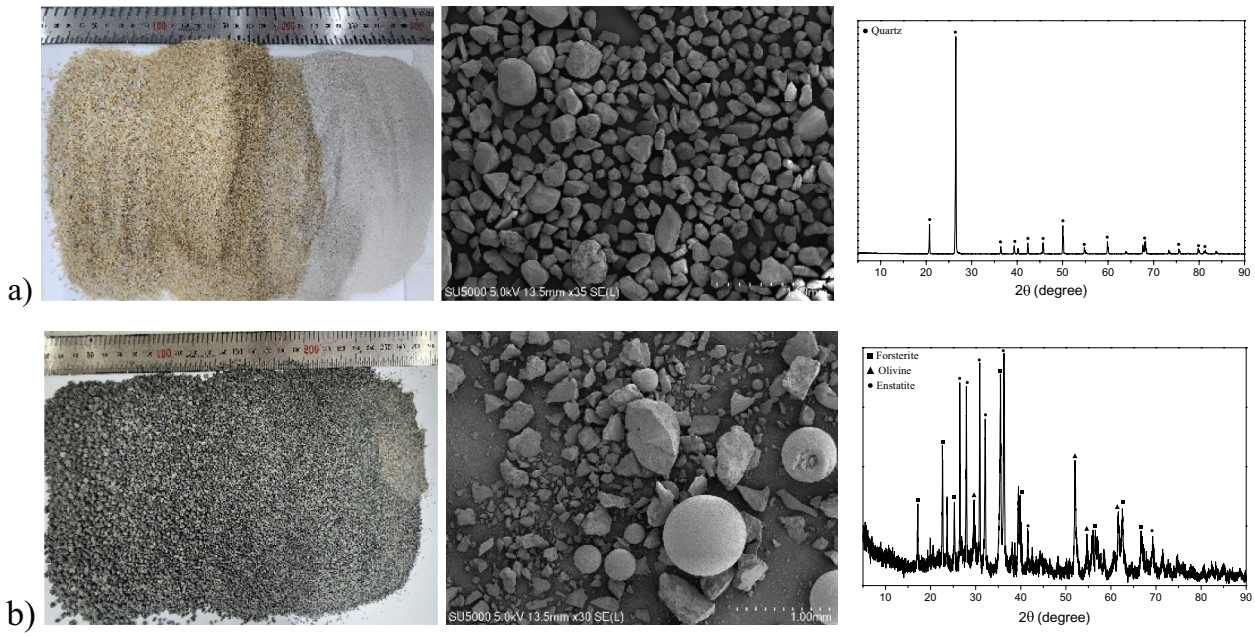

Fig. 1 **a**) Standard sand and **b**) FNS aggregate images along with characterisation

of an amorphous silica rich phase, which is known to be potentially reactive in ASR. In addition, sharp peaks corresponding to Forsterite, Enstatite, and Olivine confirm the presence of crystalline magnesium silicate phases. Figure 2 presents the particle size distribution curves of the fine aggregates used in the study. It is evident that the FNS aggregates exhibit a coarser gradation compared to the standard aggregates, with their distribution approaching the lower limit of the recommended fine aggregate size range. This variation in particle morphology, as observed in the Scanning Electron Microscopy (SEM) images and particle size distribution (Figs. 1 and

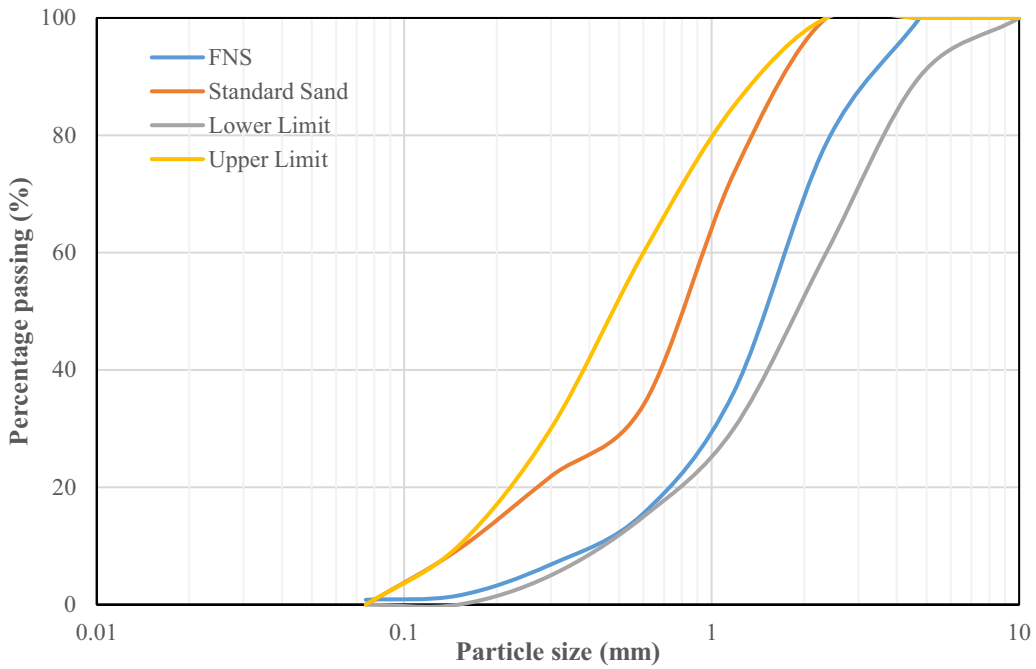

Fig. 2 Particle size distribution of materials

2), can influence the packing behaviour and mechanical properties of the resulting mortar. The differences in shape and grading between FNS aggregates and standard sand are expected to affect particle arrangement, which in turn contributes to changes in density and compressive strength of the cement composites.

3 Mix Proportion and Mix Designation

In this study, three different water to cement ratios (w/cm) of 0.35, 0.475, and 0.6 were selected to evaluate their impact on the performance and behaviour of cement mortar. The chosen w/cm ratios represent low, medium, and high levels, allowing a comprehensive assessment of mechanical properties and ASR expansion. The lowest w/cm ratio was chosen to evaluate performance under dense, low-permeability conditions, aiming to minimise ASR potential and simulate high strength applications. Conversely, the highest w/cm ratio was selected to assess behaviour in more porous, workability driven scenarios, reflecting conventional to low-strength concrete applications. These boundaries encompass a realistic range of material performance while ensuring compatibility with standard practices. Furthermore, we selected replacement levels of 0%, 50%, and 100% for FNS aggregates to focus on distinct stages of replacement: no replacement, partial replacement, and full replacement. These levels were chosen to assess the performance and behaviour of concrete with FNS aggregates under practical and industrially relevant scenarios. Partial (50%) and full (100%) replacements are critical thresholds for evaluating the feasibility and effectiveness of alternative aggregates. The mortar is prepared with FNS fine aggregates proportions of 0, 50 and 100% replaced by the weight of natural sand. Detailed information for all mixes and mix designations is provided in Table 3.

Table 3 Mix details with the mix designation used in the present study

Mix designation [*,#]	w/cm ratio	Standard Sand	FNS
L-FNS0	0.35	100%	–
L-FNS50		50%	50%
L-FNS100		–	100%
M-FNS0	0.475	100%	–
M-FNS50		50%	50%
M-FNS100		–	100%
H-FNS0	0.60	100%	–
H-FNS50		50%	50%
H-FNS100		–	100%

[*] L low w/cm ratio; M medium w/cm ratio; H high w/cm ratio

[#] FNS0, FNS50 and FNS100: denote the replacement percentages of natural sand with FNS aggregates (0%, 50% and 100%, respectively)

4 Experimental Program

4.1 Mechanical and Durability Testing

For each mix, standard cube specimens measuring 50 mm × 50 mm × 50 mm were prepared. The specimens were covered and stored in the moulds for the first 24 ± 2 h at laboratory conditions (temperature 20 ± 2 °C). After demoulding, the specimens were immediately transferred to a curing tank filled with water and stored at the same controlled temperature until the specified testing ages. At the end of each curing period, the specimens were surface dried for approximately 20–30 min at room temperature and tested for compressive strength with a uniform load application rate as prescribed by the standard. The compressive strength of the mixes was evaluated according to ASTM C109 (ASTM C109, 2021) at 3, 7, 14, 28, and 56 days. The ASR potential of the mortar mixtures was evaluated in accordance with ASTM C1260 (ASTM C, 1260 2021), commonly referred to as the Accelerated Mortar Bar Test. For each mix, mortar bars measuring 25 mm × 25 mm × 285 mm were cast using stainless steel moulds. The fresh mortar was compacted in two layers and rodded uniformly to eliminate entrapped air. The specimens were covered and stored in the moulds for the initial 24 ± 2 h at a temperature of 20 ± 2°C. After demoulding, the bars were immersed in water and stored at 80 ± 2 °C for an additional 24 h to ensure initial hydration. Following this, the specimens were immersed in a 1 N sodium hydroxide (NaOH) solution maintained at 80 ± 2 °C for the duration of the test. Length change measurements were recorded periodically using a length comparator, starting from the initial reading before immersion in NaOH. Expansion readings were taken at regular intervals up to 14 days to assess the ASR induced deformation. The average expansion values were computed from replicate specimens for each mix to ensure reliability and consistency of the results. This duration, though short in the context of long term field performance, is sufficient for screening the ASR potential of aggregates and enables comparative analysis under controlled laboratory conditions.

Further tests were extended to evaluate the behaviour of FNS fine aggregates under different environmental conditions, specifically both water and $Ca(OH)_2$ solution. The specimens were exposed to elevated temperatures of 80 ± 2 °C in both environments and their dimensional changes were monitored at regular intervals up to 14 days. This testing approach was motivated by practical considerations, particularly in cold climate regions, where floor heating systems are common. In such scenarios, hot water pipes passing through mortar floors can elevate temperatures beyond 80 °C, creating conditions similar to the $Ca(OH)_2$ environments that naturally form

within the mortar. Therefore, testing in $Ca(OH)_2$ solution simulates these elevated temperature effects and local environmental conditions, ensuring the results are applicable to real world scenarios. Furthermore, testing in $Ca(OH)_2$ solutions with wet/dry cycles was carried out to simulate the alkaline pore water chemistry typically found in concrete. Each cycle consisted of 24 h of drying at 80 ± 2 °C followed by 24 h of immersion in $Ca(OH)_2$ solution at the same temperature. These tests were performed for up to 14 days to evaluate the behaviour of FNS aggregates under cyclic environmental exposure. This approach complements the NaOH tests and provides insights into durability under realistic but less aggressive conditions. By exploring these conditions, the research provides insights into the durability and performance of FNS containing cement mortars when exposed to water, $Ca(OH)_2$ and NaOH, helping to determine their suitability for various applications.

4.2 Microstructural Characterisation

For microstructural analysis, mortar specimens which are tested for ASR expansion were used for scanning electron microscopy investigations. Samples were sectioned using a precision diamond saw to obtain smooth cross sections for imaging. To gain further insights, the fractured surfaces of ASR exposed mortars were observed, focusing on the interfacial transition zones. SEM analysis was carried out to identify ASR-related gel formation and typical hydration products. As shown in Fig. 3, the SEM/EDS samples were prepared for detailed analysis. A detailed examination was conducted, and representative micrographs are presented to highlight the key microstructural features observed in the study.

4.3 Predictive Modelling and Visualisation

To gain deeper insights into the complex interactions among these selected variables, a statistical approach was adopted. Building on previous studies that highlighted regression analysis as an effective predictive tool for material performance (Chithra et al., 2016; Tam et al., 2022). In this study, regression analysis was utilised as a predictive tool to evaluate the influence of key parameters on ASR in cement mortar containing FNS aggregates. The independent variables considered in the analysis were compressive strength at 28 days, w/cm ratio, and FNS aggregate content. These selected independent variables were chosen based on their indirect yet significant influence on ASR expansion, as demonstrated in previous studies and supported by the experimental findings in this work. The w/cm ratio affects the porosity of the matrix and the mobility of alkali ions, which are critical factors in ASR progression. The compressive strength indicates overall material densification and matrix integrity, both of which influence the extent of ASR induced expansion. Meanwhile, the FNS content directly impacts the proportion of reactive aggregates and alters both the chemical and physical characteristics of the mortar system.

To develop a predictive model for ASR expansion in cement mortar containing FNS aggregates, a stepwise regression analysis approach was adopted. The modelling process progressed through a sequence of increasingly complex functional forms to capture both linear and non-linear relationships among the selected independent variables. Initially, a simple linear regression model was developed using the following equation:

$$Y = \beta_0 + \sum \beta_i X_i \quad (1)$$

where Y is the 14-day ASR expansion, X_i are the input variables (compressive strength, w/cm ratio, and FNS content), and β_0, β_i are regression coefficients.

However, this initial model exhibited limited predictive capability, with a relatively low coefficient of determination (R^2) and statistically insignificant p values for some variables. To address this, the model was enhanced by incorporating interaction terms to account for the interdependence between input variables, resulting in a two factor interaction model using the following equation:

$$Y = \beta_0 + \sum \beta_i X_i + \sum \beta_{ij} X_i X_j \quad (2)$$

This formulation showed an improved fit, but further enhancement was necessary to fully capture the observed trends in the data. Consequently, a second-order polynomial regression model was formulated by adding quadratic terms using Eq. (3), resulting in the final model form:

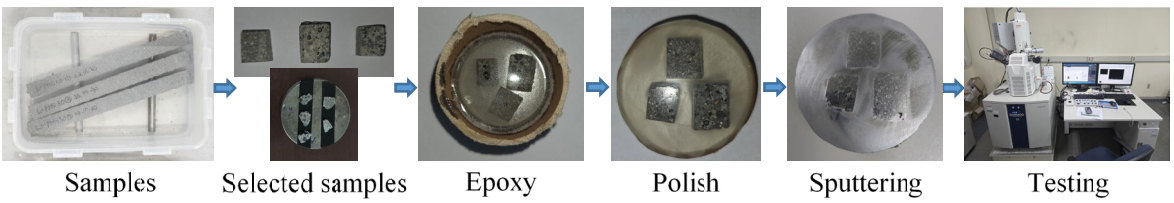

Fig. 3 Sample preparation for SEM/EDS testing

$$Y = \beta_0 + \sum \beta_i X_i + \sum \beta_{ij} X_i X_j + \sum \beta_{ii} X_i^2 \quad (3)$$

The regression coefficients were determined using the least squares method, minimising the mean square error (MSE) between predicted and experimental ASR expansion values. Statistical significance of each term was evaluated using p values (threshold: $p < 0.05$), and the overall goodness of fit was assessed using the R^2 value. The final model demonstrated excellent predictive performance with a high R^2 value; all retained variables were statistically significant. This stepwise approach allowed for progressive refinement of the model, yielding a more accurate representation of the complex relationships governing ASR expansion. (Flanders et al. 1992; Gao, 2024; Huang et al., 2010; Lokesha et al., 2023; Ruiz & Freyne, 2020; Xie et al., 2023) To further illustrate the relationships identified, 3D surface plots were generated using the regression equations. These visualisations highlight the combined effects of the independent variables on ASR under various conditions, offering a comprehensive understanding of parameter interactions.

5 Results and Discussion

5.1 Compressive Strength

The failure pattern of specimens containing FNS aggregates was comparable to that of those with natural sand, as shown in Fig. 4. All mortar specimens subjected to compressive strength testing exhibited a typical hourglass shaped failure pattern. This failure mode is indicative of axial splitting under uniaxial compressive stress and reflects uniform load distribution and consistent material behaviour across all mixes. No irregular or premature failures were observed, suggesting adequate bonding and compaction quality in the specimens.

The mean compressive strength results for all mixes were evaluated up to 56 days of curing and are presented in Fig. 5. As expected, an increase in the w/cm ratio led to a significant reduction in compressive strength, which is a well-known characteristic of cement composites (Kim et al., 2014; Popovics & Ujhelyi, 2008; Singh et al., 2015; Yiğiter et al., 2007). In this study, L-FNS0 showed higher compressive strength at 28 days, whereas at 56 days, M-FNS0 exhibited about 1.85% higher strength than L-FNS0. This variation may be attributed to factors,

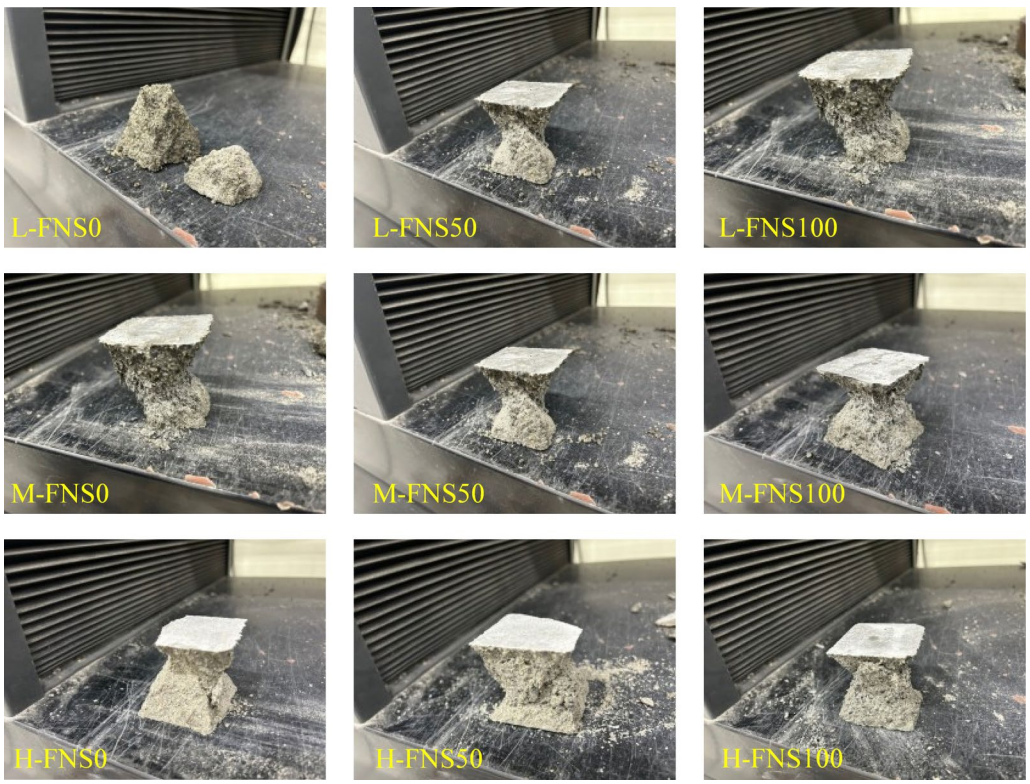

Fig. 4 Failure pattern of compressive strength cement mortar tested samples

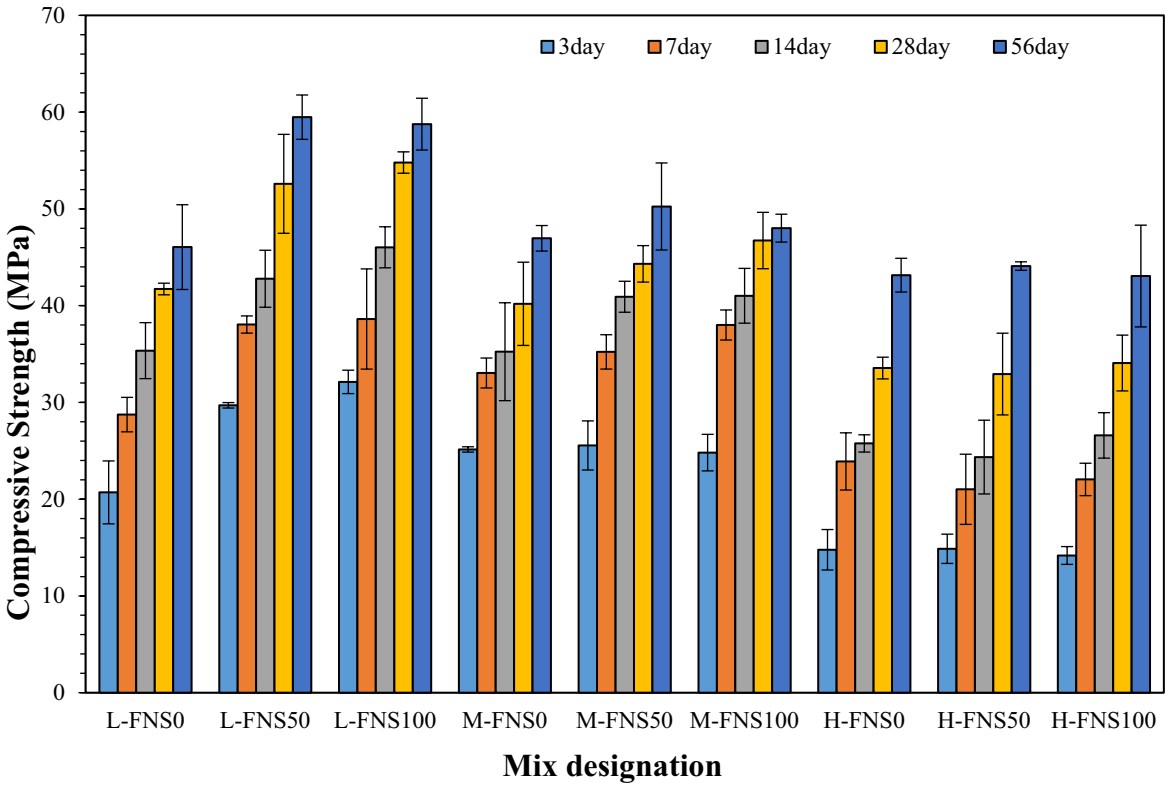

Fig. 5 Compressive strength of mortar mixes

such as improved workability and compaction in the medium w/cm ratio mix at later ages, resulting in fewer voids and a more uniform matrix. The mix L-FNS100 exhibited higher compressive strength at 28 days compared to L-FNS50. However, the highest compressive strength of 59.48 MPa was observed for the L-FNS50 mix, where 50% of the standard sand was replaced with FNS sand. The improvement in strength, particularly at 50% replacement, is primarily attributed to the optimised particle size distribution of the FNS aggregate, which contributes to better packing density and reduced voids in the matrix. This denser microstructure enhances the load bearing capacity of the mortar. The surface texture of FNS may also contribute to better mechanical interlocking at the ITZ, further improving the overall strength of the composite. This result aligns with literature reports, which identify 50% replacement of standard sand with FNS as the optimal dosage based on a combination of factors rather than strength alone (Bao et al., 2021; Saha & Sarker, 2017b, 2018).

Despite the higher w/cm ratio, compressive strength increased over time, with strength development remaining robust. The highest compressive strengths observed at 56 days were 50.25 MPa for the M-FNS50 mix and 44.09 MPa for the H-FNS50 mix. The data indicates that strength development slowed as the w/cm ratio increased, with final strengths reaching 84.5% and 74.13% of the maximum strength for the medium and high w/cm mixes, respectively. At higher w/cm, the matrix tends to be more porous and less dense, which dominates the strength behaviour of the mortar. In such conditions, the influence of aggregate properties becomes less pronounced, and the compressive strength is primarily governed by the high paste content and reduced bonding efficiency. A similar phenomenon with FNS aggregates has also been reported in the literature (Nuruzzaman et al., 2022; Saha & Sarker, 2017b).

5.2 Determination of Mortar Expansion

The ASR expansions of the mortars made with a cement binder with two types of aggregates and combinations as defined in Table 3 and the results are presented in Fig. 6. The mortar specimens with the reactive sand mixture displayed significant ASR expansion. This study used FNS aggregates, known for their reactive nature as reported in the literature (Choi & Choi, 2015; Nuruzzaman et al., 2022; Saha et al., 2018; Saha & Sarker, 2016, 2018, 2020; T. Yang et al., 2020). According to ASTM C1260, the 14-day ASR expansion of cement mortar mixes with different w/cm containing the standard sand showed well below the

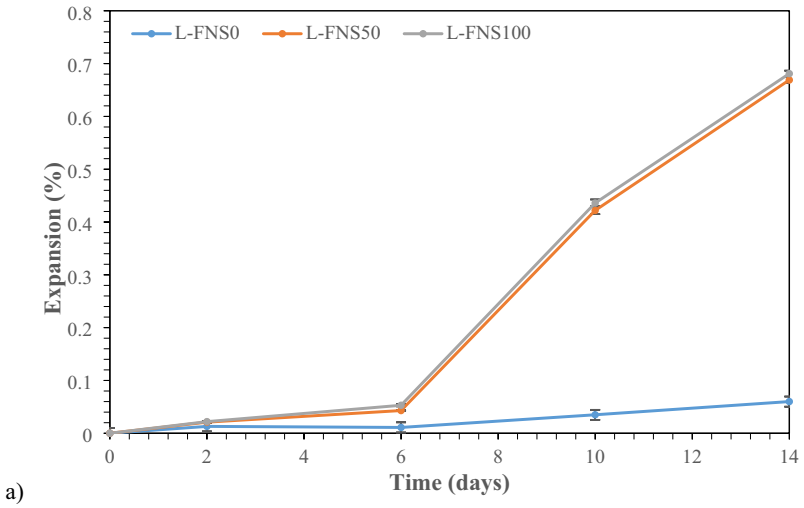

a)

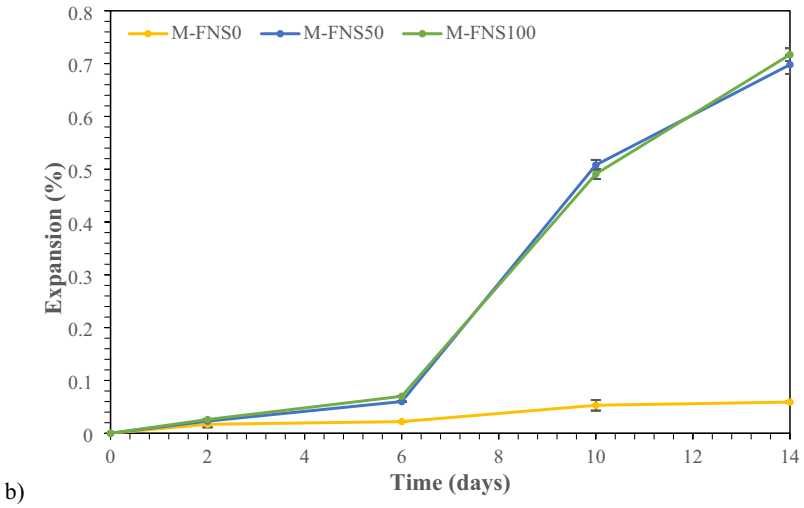

b)

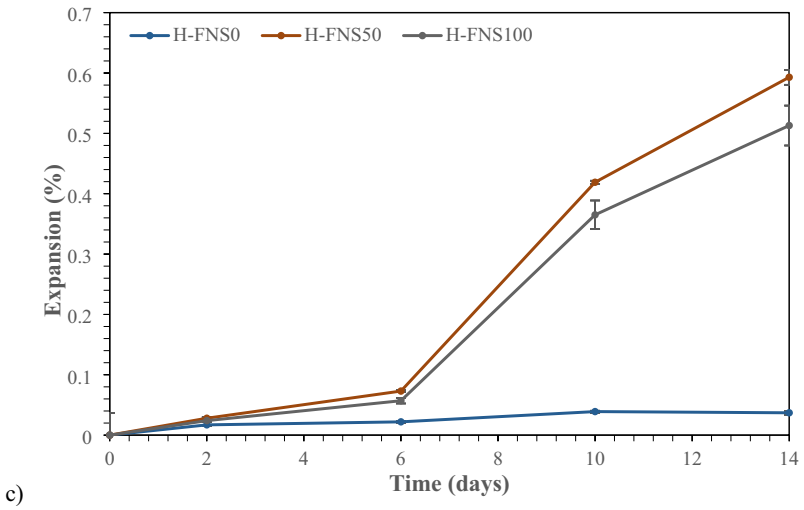

c)

Fig. 6 ASR expansion for mixes (**a**) low, (**b**) medium, and (**c**) high w/cm mixes in NaOH at 80 °C

standard's critical expansion limit of 0.1% (Fig. 6a). However, expansions increased significantly with the inclusion of FNS in the mixes, regardless of the level of FNS aggregate replacement or the w/cm. The most significant observation (Fig. 6b, c) was that the expansion of specimens containing FNS progressed at a slower rate up to 6 days, after which the rate of expansion accelerated significantly, continuing to increase at a higher pace until 14 days. This indicates that while initial ASR activity with FNS is relatively moderate, it becomes more pronounced over time, with expansion rates increasing substantially as the reaction progresses. With a 50% replacement of standard sand by FNS, ASR expansion was observed in the range of 0.593% to 0.698%. However, when standard sand was completely replaced with FNS, the ASR expansion increased further, ranging from 0.513% to 0.717%. Furthermore, it is to be noted that the mixes (H-FNS50 and H-FNS100) with higher w/cm had lower ASR expansion when compared to mixes (L-FNS50, L-FNS100, M-FNS50 and M-FNS100) with lower w/cm. The reduced ASR expansion in the H-FNS mixes can be attributed to the higher w/cm, which increases the porosity of the cement matrix. Increased porosity allows for better dissipation of internal stresses caused by ASR, thus limiting expansion. In contrast, M-FNS mixes, despite having a medium w/cm, exhibited greater porosity than L-FNS mixes, allowing increased transportation of alkali ions. This facilitated more ASR in M-FNS compared to L-FNS, where the denser matrix and lower porosity restricted NaOH penetration, resulting in comparatively less ASR expansion. This indicates that ASR in FNS mortars was highly reactive when submerged in NaOH solution, likely due to the significant ingress of external sodium hydroxide respective of w/cm.

As explained in Sect. 4, expansions were investigated in $Ca(OH)_2$ environments to gain a deeper understanding of the behaviour of FNS aggregates in cold climate regions, stemming from practical applications. This study aimed to assess the interaction between FNS aggregates and calcium hydroxide, focusing on their potential reactivity and stability in such conditions. M-FNS mortar mixes were subjected to $Ca(OH)_2$ at 80 °C, with the results presented in Fig. 7. During the initial period, minimal expansion was observed, ranging from 0.019% to 0.022% up to 8 days, followed by noticeable shrinkage between 0.006% and 0.017%. By 14 days, all mixes showed little to no further expansion or shrinkage, indicating a stabilising effect due to the $Ca(OH)_2$ environment at 80 °C. The differences in ASR behaviour between the NaOH and $Ca(OH)_2$ environments can be attributed to the dissociation properties of these compounds. NaOH fully dissociates in water, leading to a higher concentration of hydroxide ions, which accelerates the ASR process and results in greater expansion. In contrast, $Ca(OH)_2$ only partially dissociates, resulting in a lower concentration of hydroxide ions. This leads to slower reactivity, as evidenced by the minimal expansion and subsequent stabilisation or shrinkage in the M-FNS mortar mixes exposed to $Ca(OH)_2$ at 80 °C.

The expansion was further investigated in $Ca(OH)_2$ at 80 °C under wet and dry cycles for 14 days, with

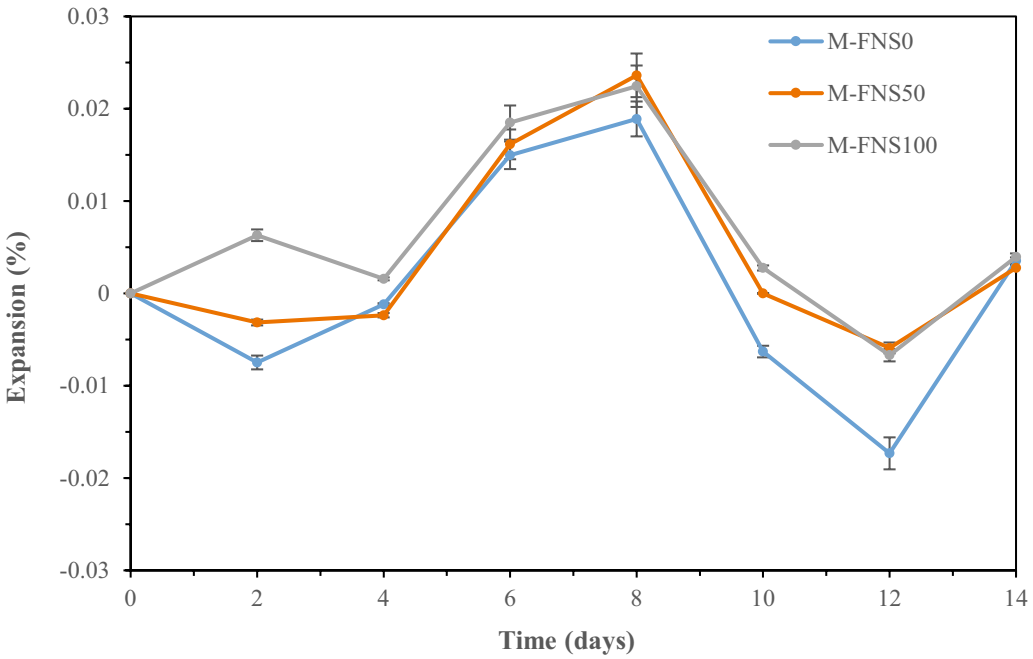

Fig. 7 Expansion M-FNS in $Ca(OH)_2$ 80 ℃

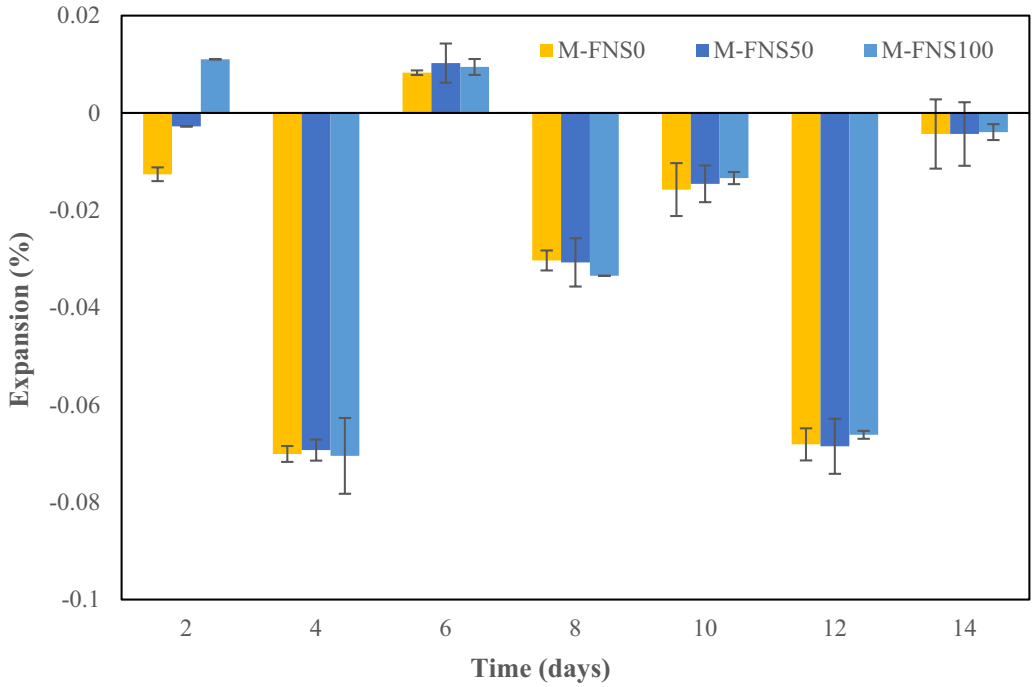

Fig. 8 ASR expansion M-FNS in $Ca(OH)_2$ 80 ℃ wet and dry cycles

results presented in Fig. 8. During the drying phases, the specimens exhibited noticeable shrinkage due to moisture loss. However, during subsequent wetting cycles, the specimens partially regained their original length, indicating some reversibility of the shrinkage. By the end of the 14 days, the specimens experienced nearly negligible and very low shrinkage. The alternating wet and dry exposure conditions likely delayed the reactivity of the FNS aggregates, thus reducing its impact when subjected to $Ca(OH)_2$ at 80 °C.

In addition, the ASR expansion of the M-FNS100 mix was studied in water at 80 °C and compared with standard ASR results in NaOH and $Ca(OH)_2$. The experimental results, presented in Fig. 9, indicate that neither water nor $Ca(OH)_2$ environments induced any noticeable expansion in the cement mortar containing FNS aggregates. This can be attributed to the very low alkali content in the mix, as confirmed by the chemical composition of both the cement and the FNS aggregates, which showed negligible levels of reactive alkalis necessary to initiate the ASR process. In contrast, the NaOH solution led to significant expansion, exceeding the ASTM limits. This highlights the higher reactivity of FNS aggregates in a highly alkaline environment like NaOH, while the relatively neutral or mildly alkaline environments of water and $Ca(OH)_2$ did not trigger any expansion.

6 Scanning Electron Microscope Studies

After testing ASR mortar samples for expansion, they were brought into a suitable form to examine their microstructures through a SEM. SEM analysis focused on the interfacial regions around the aggregates in cross sections of ASR tested mortar samples with varied w/cm ratios, as shown in Fig. 10. While the EDS results confirm the presence of typical hydration products and some ASR-related features, identifying ASR expansion and its characteristics in the cross-sectional specimens proved somewhat difficult and limited. Therefore, fractured specimens were examined in detail to better observe ASR-related formations, as shown in Figs. 11 and 12. EDS analysis was also conducted, and the corresponding weight percentages are presented in Table 4. Sample L-FNS0, as shown in Fig. 11a, illustrates the interface between dense hydration products and sand grain, indicating the absence of ASR formation, since the sample does not contain and reactive silica. In Fig. 11b, and (c, the samples containing FNS aggregates, specifically M-FNS50 and H-FNS100, exhibit a porous, web-like or interconnected network structure, indicative of ASR product formation (Doğruyol, 2024; Gholizadeh Vayghan et al., 2016; Z. Shi et al., 2015). These crystalline structures can be observed around and on the surface of the FNS aggregates, indicating a reaction between the alkalis and the reactive silica present in the FNS. The presence of these crystalline products

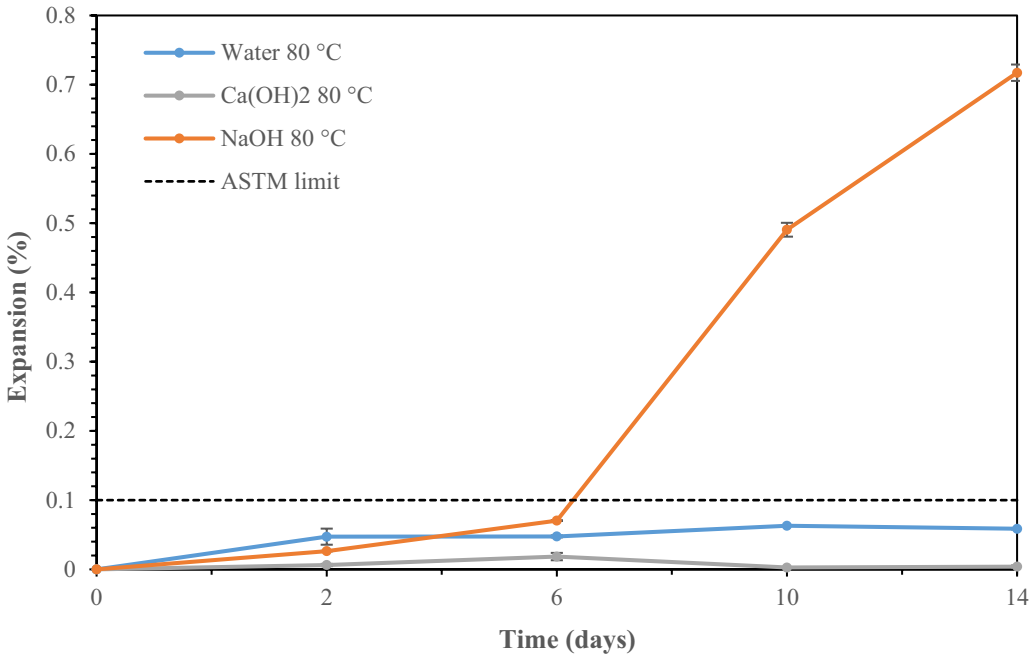

Fig. 9 ASR expansion M-FNS100 with different environments

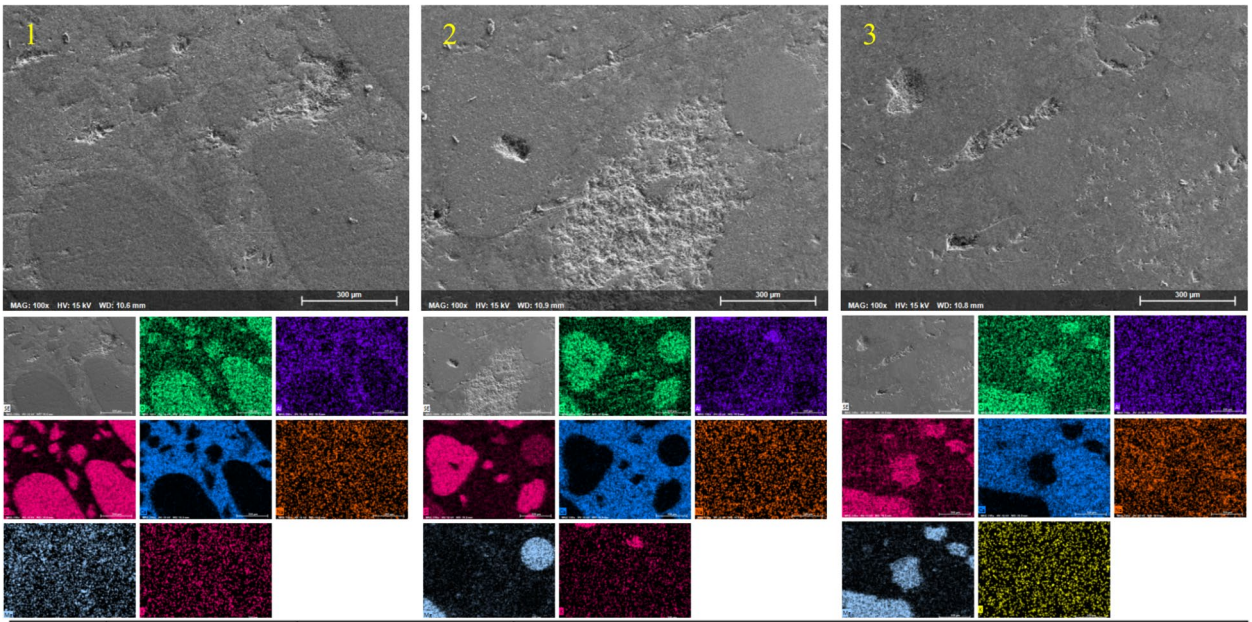

Sl. No.	Sample designation	Environment	ω_t (%)						
			O	Ca	Si	Al	Na	K	Mg
1	L-FNS0	NaOH	42.98	19.43	35.13	1.22	0.41	0.16	0.66
2	M-FNS50	NaOH	42.94	24.71	26.70	1.82	0.17	0.17	3.49
3	H-FNS100	NaOH	42.80	28.10	16.23	2.08	2.47	0.17	8.14

Fig. 10 SEM and EDS around the FNS aggregates in smooth surface ASR mortar sample

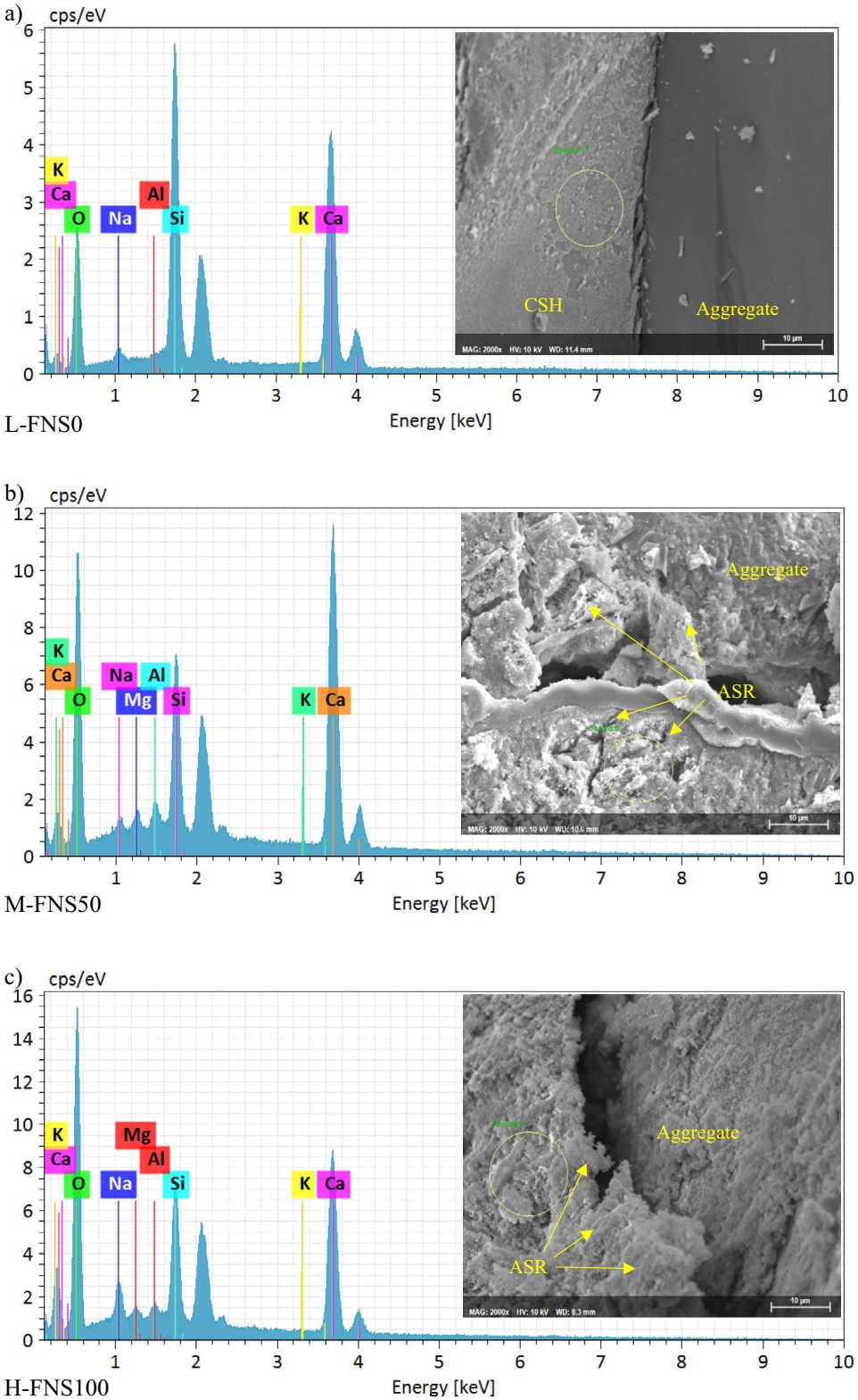

Fig. 11 SEM and EDS around the FNS aggregates in broken surface ASR mortar sample **a**) L-FNS0 **b**) M-FNS50 **c**) H-FNS100

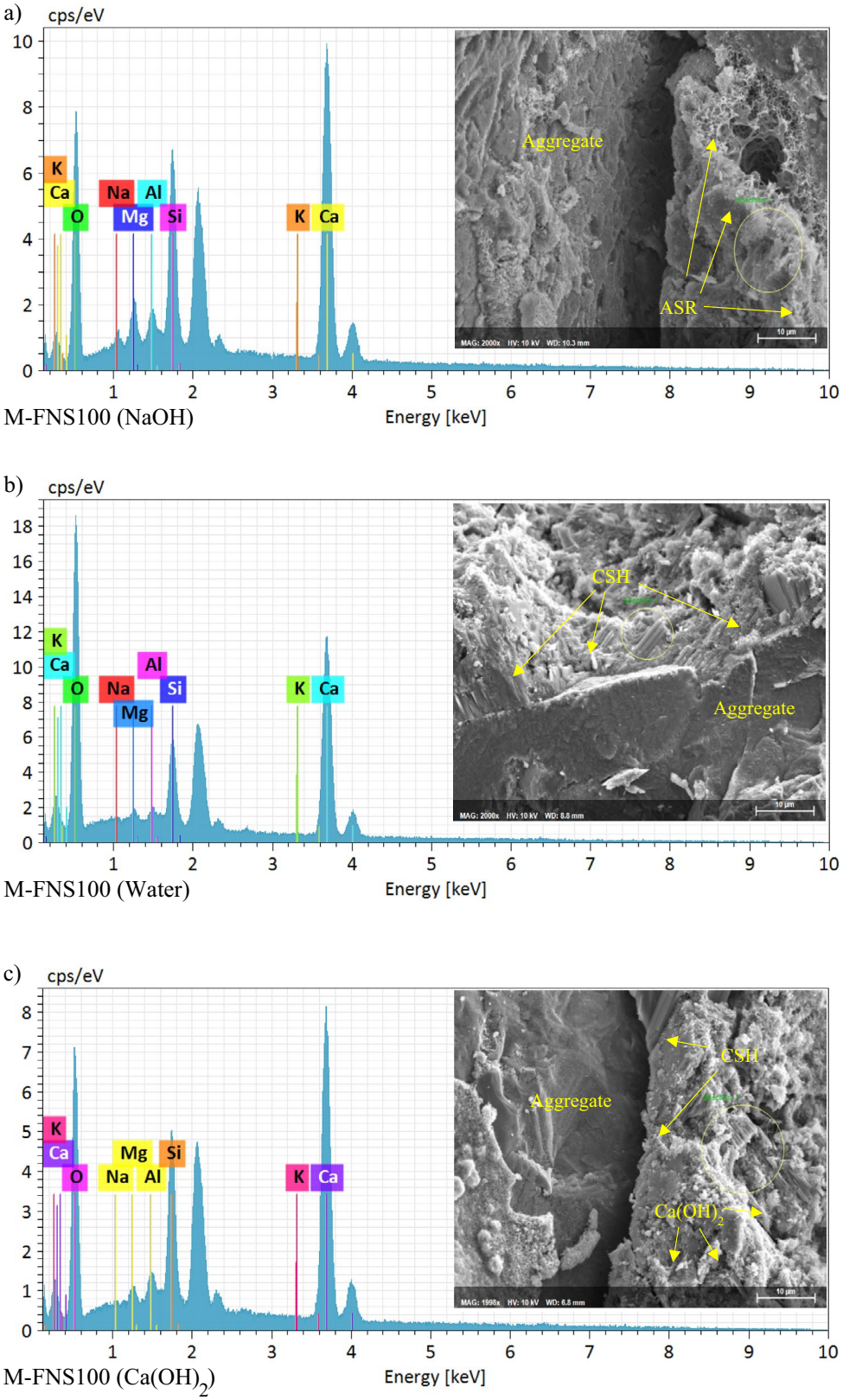

Fig. 12 SEM and EDS around the FNS aggregates in mortar M-FNS100 samples from different environments **a**) NaOH **b**) Water **c**) Ca(OH)2 **d**) Ca(OH)2 w/d

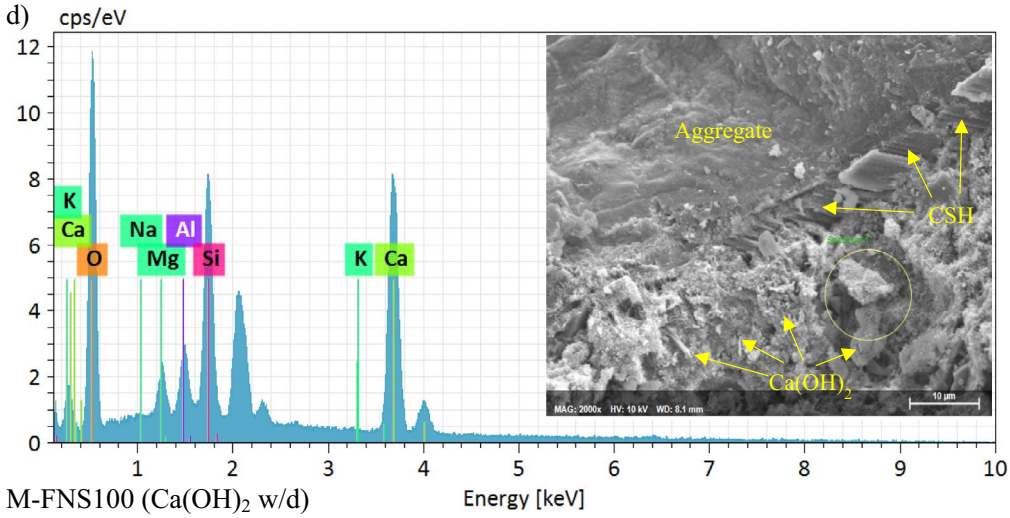

Fig. 12 continued

Table 4 Element mass from EDS analysis

Sample designation	Environment	ω_t (%)						
		O	Ca	Si	Al	Na	K	Mg
L-FNS0	NaOH	29.80	45.03	23.55	0.23	0.81	0.59	–
M-FNS50	NaOH	42.54	46.29	9.06	0.63	0.49	0.14	0.55
H-FNS100	NaOH	51.23	36.52	9.27	0.60	2.01	0.03	0.34
M-FNS100	NaOH	37.81	47.46	10.73	1.38	0.57	0.35	1.70
M-FNS100	Water	53.43	39.09	5.76	0.57	0.58	0.08	0.46
M-FNS100	$Ca(OH)_2$	41.73	47.35	9.25	1.16	–	0.10	0.42
M-FNS100	$Ca(OH)_2$ w/d	46.67	36.89	12.42	2.47	0.02	0.09	0.23

suggests that ASR activity has occurred, leading to the formation of expansive gel, which can potentially cause micro cracking in the cement matrix. Based on the EDS analysis and Table 4, the presence of Si, Na, and K indicates the potential formation of ASR gel, which is likely responsible for the observed porous and network-like structures.

In Fig. 12a, sample M-FNS100 exposed to NaOH at 80 °C, a porous, interconnected network of filaments or web-like formations, indicative of ASR products, is observed. Figure 12b shows that the M-FNS100 sample, which contains 100% FNS aggregates, did not exhibit ASR-related products when exposed to water at 80°C. This suggests that the FNS aggregates remain stable in water, likely due to the minimal formation of an alkali environment or delay the initiation. The absence of product-related ASR highlights the influence of alkaline solutions, like NaOH, in triggering ASR, as opposed to water alone. Furthermore, in Fig. 12c, d, the MFNS100 sample exposed to the $Ca(OH)_2$ environment and the $Ca(OH)_2$ wet/dry cycles exhibited no evidence of ASR product formation. Instead, substantial deposits of calcium hydroxide were observed at the interface between the FNS aggregates and the cement matrix (Lei et al., 2021). This suggests that the $Ca(OH)_2$ environment will not facilitate any reactivity of FNS aggregates, as further supported by the EDS analysis and data from Table 4.

7 Regression Analysis and Predictive Modelling

From the experimental study results and characterisation of the samples, it is evident that the presence of FNS aggregates in the cement matrix creates a critical scenario that magnifies the ASR activity when exposed to a NaOH environment. This intensified reactivity leads to significant detrimental effects on the material's stability and performance. Instead of conducting repetitive experimental work, predictive equations can be utilised. In this context, regression analysis, as explained in Sect. 4.3, was performed to develop such predictive models. To predict the ASR at 14 days in cement mortar containing FNS

aggregates, regression analysis was performed using the experimental data. The independent variables considered in the analysis included compressive strength at 28 days, w/cm and FNS aggregate content. This regression model aims to establish a relationship between these variables and the ASR, providing a predictive tool for future studies and applications.

Based on the experimental data, the regression analysis was performed with linear fit considering compressive strength at 28 days, w/cm and FNS aggregate content. The linear regression analysis showed that a positive correlation between the parameters and ASR expansion could not be established. The low R-squared value (0.743) and high *p* values for compressive strength (0.134) and w/cm (0.451) suggest that these variables do not significantly impact ASR expansion in a linear model (Gao, 2024; Xie et al., 2023). This indicates that the relationships are likely more complex and may involve interaction effects or non-linear behaviour, which a simple linear fit cannot capture. However, FNS aggregate content (1.989×10^{-5}) showed a significant influence, affirming further investigation. Linear fitting was applied to individual parameters and their combinations, and the results are summarised in Table 5. The analysis showed that all three parameters compressive strength, w/cm ratio, and FNS aggregate content play a significant role in some cases in predicting ASR expansion.

Furthermore, interaction terms were incorporated into the regression model, resulting in an improved R-squared value of 0.807 compared to the previous model. Linear fitting was then applied, including interaction terms to individual parameters and their combinations, with the results summarized in Table 5. The table demonstrates that the inclusion of interaction terms significantly influences the prediction of ASR activity. To enhance the predictive accuracy, interaction terms and second-degree terms were included to account for non-linear relationships and interactions among the variables in the next stage of the regression model (Flanders et al. 1992; Huang et al., 2010; Wu et al., 2024). The R-squared value increased to 0.995, indicating a high level of accuracy in predicting ASR activity based on the selected parameters. Out of the 9 parameters, 7 showed a significant influence in predicting ASR activity. However, the interaction term between compressive strength and FNS aggregate and the second-order w/cm ratio did not contribute meaningfully to the model. Therefore, regression analysis excluded these two terms, resulting in a regression model with an R-squared value of 0.995. All remaining parameters are statistically significant in predicting ASR activity, and the equation is presented below:

$$\begin{aligned} \mathrm{ASR} = {} & 3.301 - 0.103(\mathrm{CS}) - 4.474(\mathrm{w/cm}) \\ & + 0.024(\mathrm{FNS}) + 0.109(\mathrm{CS} \times \mathrm{w/cm}) \\ & - 0.010\,(\mathrm{w/cm} \times \mathrm{FNS}) + 5.894 \times 10^{-4}\left(\mathrm{CS}^2\right) \\ & - 1.305 \times 10^{-4}\left(\mathrm{FNS}^2\right) \end{aligned} \tag{4}$$

Table 5 R-squared values and *p* values for regression analysis parameters

R-square	*p* value								
	CS	w/cm	FNS	CS x w/cm	CS x FNS	w/cm x FNS	$(CS)^2$	$(w/cm)^2$	$(FNS)^2$
0.743	0.134	0.451	1.989×10^{-5}						
0.220	0.014								
0.018		0.510							
0.698			5.829×10^{-8}						
0.424	3.980×10^{-4}	7.680×10^{-3}							
0.716		0.235	6.458×10^{-8}						
0.433	3.230×10^{-4}		0.539						
0.807	0.685	0.821	0.014	0.402	0.019	0.041			
0.743	0.558	0.789	3.851×10^{-5}	0.969					
0.759	0.062	0.336	0.034		0.233				
0.743	0.204	0.470	0.374			0.903			
0.761	0.254	0.553	0.037	0.748	0.227				
0.743	0.585	0.763	0.473	0.918		0.878			
0.800	0.016	0.076	0.016		0.024	0.053			
0.995	0.062	0.168	4.763×10^{-4}	0.055	0.456	0.047	0.084	0.534	5.162×10^{-15}
0.995	1.196×10^{-3}	6.550×10^{-5}	2.084×10^{-15}	4.865×10^{-5}		3.483×10^{-6}	8.899×10^{-3}		6.914×10^{-18}

where ASR—alkali silica reaction prediction at 14 days, CS—compressive strength of cement mortar at 28 days, w/cm—water-to-cement ratio used in the preparation of cement mortar, FNS—ferronickel slag aggregates content in the cement mortar.

Following the regression analysis, 3D plots were generated using Eq. 4 to visually represent the relationship between the key parameters such as compressive strength, w/cm ratio, and FNS aggregate content and the predicted ASR expansion at 14 days. These visualisations allow for a clearer understanding of how the interaction between these variables influences ASR activity in cement composite.

Figure 13 presents a 3D surface plot that demonstrates the relationship between predicted ASR expansion at 14 days, compressive strength and w/cm, with two distinct conditions: 0% FNS (no FNS aggregate replacement) and 100% FNS (complete replacement of natural aggregates with FNS). The contours and surface levels clearly depict the interaction of these variables and their combined influence on ASR behaviour. For the 0% FNS replacement, the ASR values tend to remain higher, especially at higher w/cm and lower compressive strengths. This clear shows that their is a higher susceptibility to ASR in mixes without FNS, as some natural aggregates are reactive.

In contrast, with 100% FNS replacement, the ASR levels are substantially high, indicating that the addition of FNS significantly contributes to ASR expansion. The plot reveals that mixes with lower w/cm ratios and higher compressive strength exhibit minimal ASR expansion in both scenarios. Overall, this figure emphasises the dual role of optimising the w/cm ratio and utilising FNS replacement to suppress ASR while maintaining favourable compressive strength levels. It highlights the effectiveness of FNS as a sustainable alternative material.

Figure 14 presents a 3D surface plot highlights the combined influence of FNS aggregate content and compressive strength on ASR expansion at 14 days, under two distinct w/cm: low (0.35) and high (0.6). For a low w/cm ratio, ASR expansion is consistently lower across all FNS aggregate content levels, reflecting the reduced water availability, which limits alkali mobility and reduces ASR reaction kinetics. As FNS aggregate content

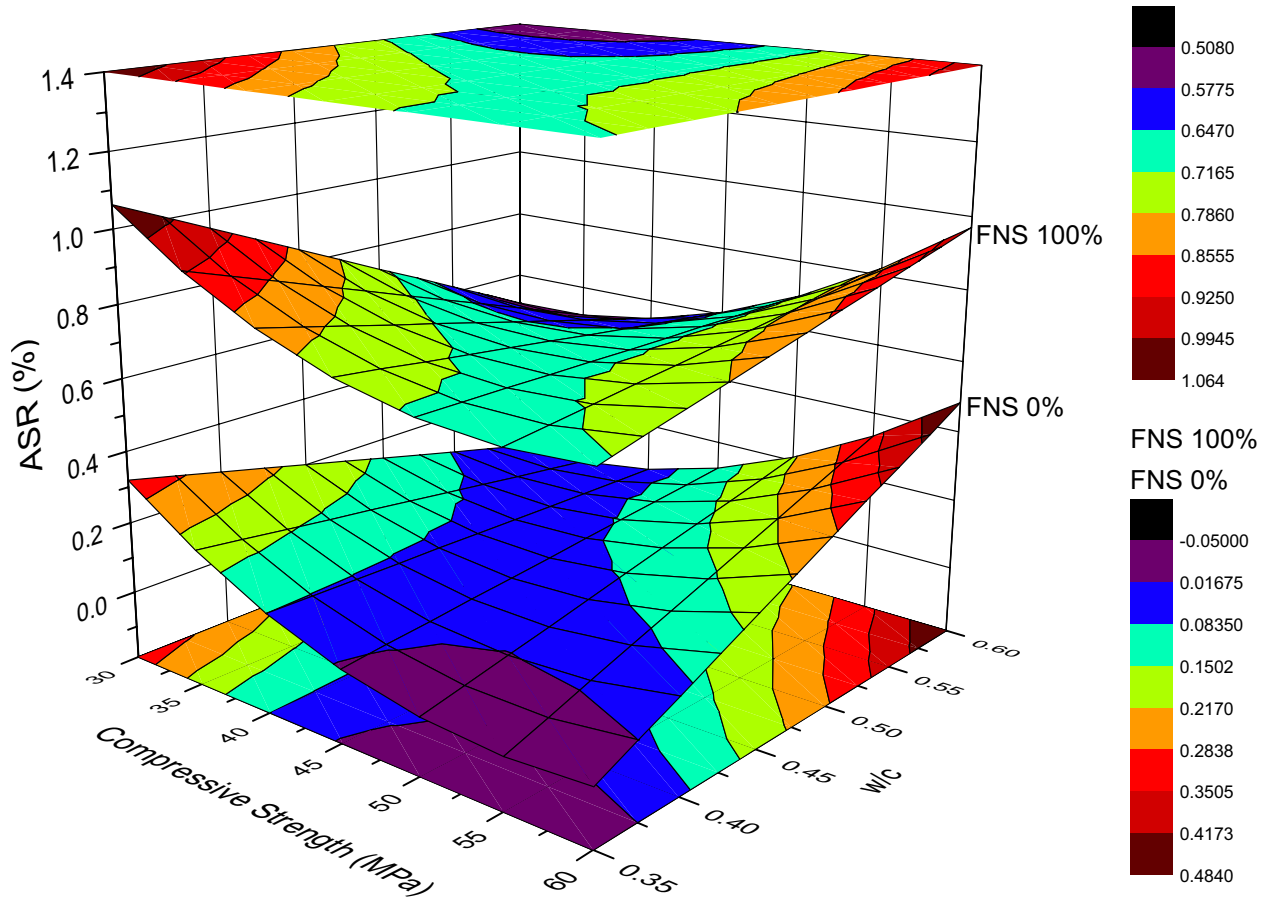

Fig. 13 Predicted ASR at 14 days as a function of compressive strength and w/cm at 0% and 100% FNS aggregate content

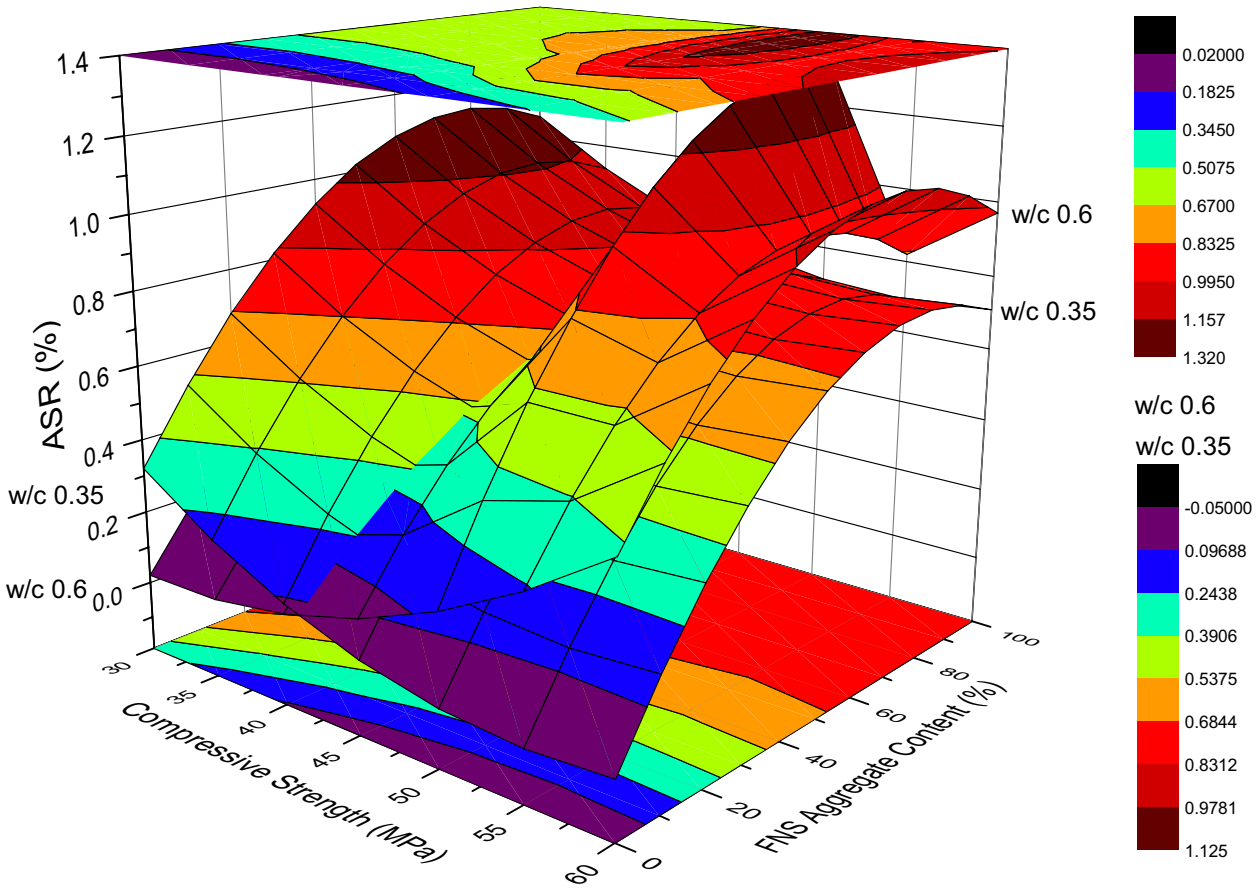

Fig. 14 Predicted ASR at 14 days as a function of compressive strength and FNS aggregate content at fixed w/cm (0.35 and 0.6)

increases, a notable reduction in ASR is observed, particularly at higher compressive strength levels. This behaviour indicates that at a lower w/cm ratio, the influence of FNS aggregates on ASR expansion becomes more pronounced.

At a high w/cm ratio, the ASR levels are significantly elevated due to increased pore water availability, facilitating ASR reactions. However, even at this high w/cm ratio, an increase in FNS aggregate content shows a clear reduction in ASR expansion. However, the effect is less pronounced compared to the low w/cm ratio condition. This figure underscores the synergy between optimizing FNS aggregate content and maintaining a low w/cm ratio to control ASR while also achieving favourable compressive strength. It demonstrates the potential of FNS as an effective supplementary aggregate to mitigate ASR, particularly under controlled water conditions.

Figure 15 presents a 3D surface plot illustrates the influence of the w/cm ratio and FNS aggregate content on ASR expansion at 14 days, under compressive strength conditions of 30 MPa and 60 MPa. For the lower compressive strength, ASR expansion is higher at higher w/cm ratios with an increase in FNS aggregates. This is attributed to the increased porosity and pore water availability in lower strength composite, which facilitates ASR. However, a progressive reduction in ASR is observed as FNS aggregate content decreases, indicating FNS's ability to reduce ASR even in low strength mixes. For higher compressive strength, the ASR levels are generally lower, primarily due to the reduced porosity and improved densification of the matrix. At this higher strength level, increasing FNS aggregate content further suppresses ASR expansion, particularly at lower w/cm ratios. This demonstrates the effectiveness of FNS in improving durability by reducing ASR susceptibility in high strength composites. Overall, the figure emphasizes the interaction between w/cm ratio, FNS aggregate content, and compressive strength. It suggests that combining low w/cm ratios with increased FNS aggregate content is particularly effective in mitigating ASR expansion, regardless of the strength level.

These 3D surface plots offer a visual representation of the regression model, helping to better understand how selected parameters such as compressive strength, w/cm

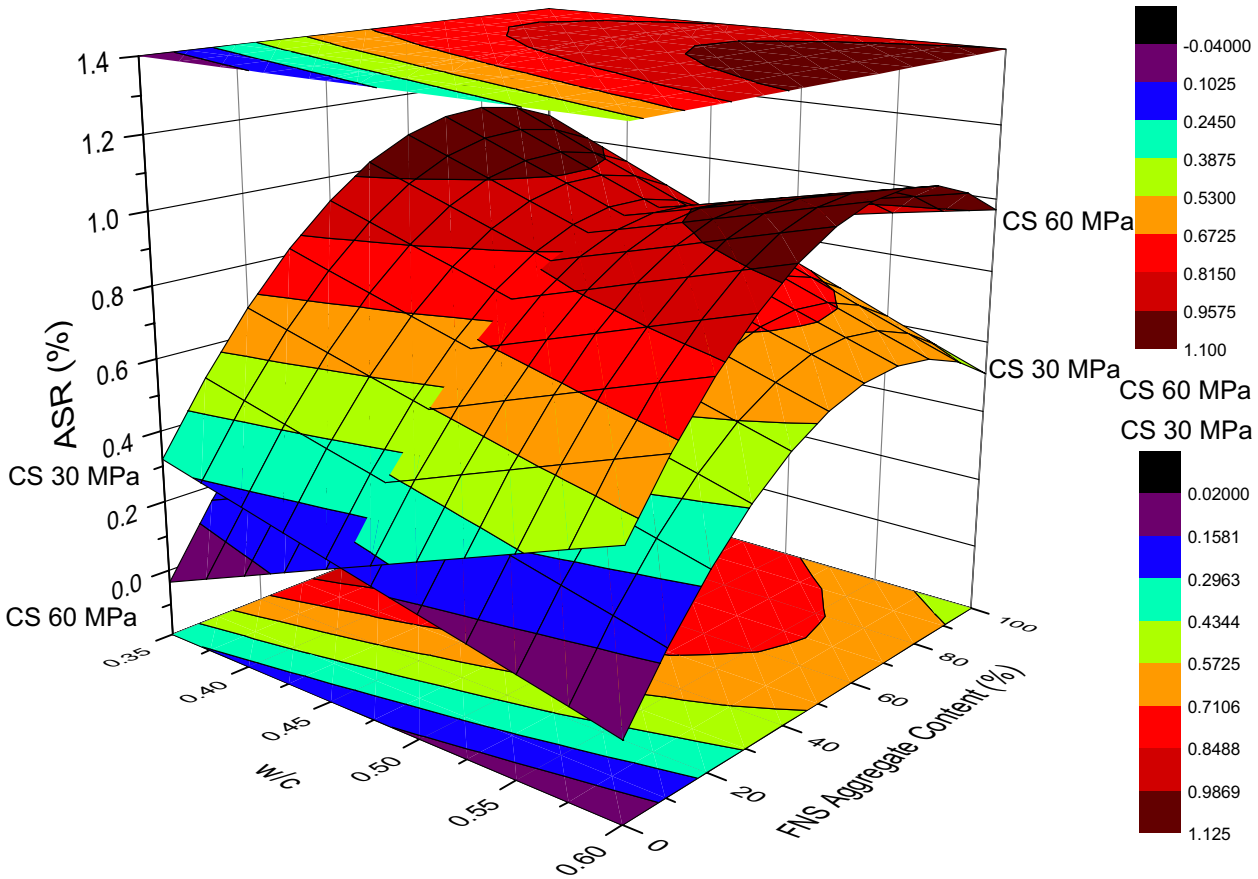

Fig. 15 Predicted ASR at 14 days as a function of w/cm and FNS aggregate content at compressive strengths of 30 and 60 MPa

ratio, and FNS aggregate content interaction and influence on ASR expansion, particularly in mixes containing highly reactive aggregates. Unlike numerical equations alone, these visualisations provide intuitive insights into complex variable interdependencies and trends, making it easier to observe critical patterns and potential thresholds affecting ASR behaviour. This graphical approach enhances the interpretability of the model, especially for practical applications and decision making in material selection and mix design.

8 Conclusion

This study presents a comprehensive evaluation of ferronickel slag waste as a sustainable fine aggregate in cement mortar, with a specific focus on its mechanical performance and susceptibility to ASR. A key finding is that a 50% replacement of natural sand with FNS optimally improved the particle size distribution, resulting in enhanced compressive strength. The influence of w/cm ratio was also evident, as higher ratios led to reduced compressive strength due to increased porosity.

ASR testing revealed that FNS aggregates are reactive in high alkali environments, particularly under accelerated conditions in NaOH at 80°C. Expansion exceeded ASTM C1260 limits, highlighting their susceptibility. Interestingly, initial ASR expansion was slower in mixes with FNS, followed by rapid growth after 6 days, suggesting delayed gel formation. Variations in w/cm ratio influenced ASR behaviour: higher porosity in high w/cm mixes allowed gel accommodation, reducing visible expansion, while lower porosity in low w/cm mixes restricted alkali ingress, mitigating ASR. In contrast, negligible ASR expansion was observed under water and $Ca(OH)_2$ exposure, including cyclic wetting–drying regimes, indicating environment-dependent reactivity.

The study further advances knowledge by developing a high accuracy regression model ($R^2 = 0.995$) for predicting ASR expansion based on compressive strength, w/cm ratio, and FNS content. The model incorporated interaction and non-linear terms, offering quantitative insight into complex parameter interdependencies. 3D response surface plots effectively visualised these relationships, reinforcing the model's interpretability. These tools provide a predictive framework to guide optimal mix design and ASR mitigation strategies, supporting

the broader goal of safe and sustainable integration of FNS in cementitious composites.

9 Limitations and Future Research

While this study offers meaningful insights into the ASR behaviour of cement mortars incorporating FNS aggregates, certain limitations must be acknowledged. The use of mortar specimens, rather than full concrete samples, limits the direct applicability of findings to field conditions, where aggregate gradation, size, and interfacial zones play more complex roles. The ASR expansion was evaluated only up to 14 days in accordance with ASTM C1260, an accelerated test method that may not capture the full long term behaviour of ASR progression. In addition, the regression model was developed using a relatively limited data set and involved predicting 14-day ASR based on 28-day compressive strength, which introduces a temporal inconsistency, given that strength development and ASR mechanisms evolve differently. Despite these limitations, the study offers a foundation for further research. Future investigations should consider long term ASR monitoring, testing on concrete specimens, and broader data sets for robust predictive modelling. Incorporating leaching studies under different chemical exposures will also help assess ion release and reactivity of FNS aggregates. In addition, exploring mitigation strategies using supplementary cementitious materials may enhance ASR resistance while supporting sustainable use of industrial by products.

Acknowledgements
This work was partly supported by the Technology Development Program of MSS [S3431827] and the ICT development R&D program of MSIT [No. RS-2023-00217322].

Author Contributions
Tae Yeon Kim: conceptualization, data curation, visualization, methodology, investigation, formal analysis, writing—original draft and writing—review and editing. Sun Gyu Park: conceptualization, supervision and writing—review and editing. Woo Jin Lee: conceptualization, visualization, methodology and writing—review and editing. Jae Hun Jung: methodology, investigation and formal analysis. Jun Chul Yoon: methodology, investigation and formal analysis. Kadepalli Nagendra Shivaprasad: conceptualization, data curation, visualization, methodology, supervision, formal analysis, writing—original draft and writing—review and editing. Hyun Min Yang: conceptualization, data curation, visualization, supervision, funding acquisition and writing—review and editing.

Data Availability
The data and materials are included in the manuscript.

Declarations

Ethics Approval and Consent to Participate
Not applicable.

Consent for Publication
Not applicable.

Competing Interests
The authors declare that they have no known competing financial interests or personal relationships that could have appeared to influence the work reported in this paper.

Received: 16 February 2025 Accepted: 16 July 2025
Published: 23 October 2025

References

Akiyama, A., & Yamamoto, Y. (1986). Utilization of ferro-nickel slag as fine aggregate for concrete. *Doboku Gakkai Ronbunshu, 1986*(366), 103–112. https://doi.org/10.2208/JSCEJ.1986.366_103

Aslani, F., Yu, J., Zhang, Y., & Valizadeh, A. (2023). Development of prediction models for evaluation of alkali-silica reaction in concrete. *Case Studies in Construction Materials*. https://doi.org/10.1016/j.cscm.2023.e02465

ASTM C109. (2021). Standard Test Method for Compressive Strength of Hydraulic Cement Mortars, 1–7.

ASTM C1260. (2021). Standard Test Method for Potential Alkali Reactivity of Aggregates, 1–5.

Bao, J., Yu, Z., Wang, L., Zhang, P., Wan, X., Gao, S., & Zhao, T. (2021). Application of ferronickel slag as fine aggregate in recycled aggregate concrete and the effects on transport properties. *Journal of Cleaner Production*. https://doi.org/10.1016/j.jclepro.2021.127149

Bartzas, G., & Komnitsas, K. (2015). Life cycle assessment of ferronickel production in Greece. *Resources, Conservation and Recycling, 105*, 113–122. https://doi.org/10.1016/J.RESCONREC.2015.10.016

Bulteel, D., Garcia-Diaz, E., Vernet, C., & Zanni, H. (2002). Alkali–silica reaction. *Cement and Concrete Research, 32*(8), 1199–1206. https://doi.org/10.1016/S0008-8846(02)00759-7

Chithra, S., Senthil Kumar, S. R. R., Chinnaraju, K., & Alfin Ashmita, F. (2016). A comparative study on the compressive strength prediction models for high performance concrete containing nano silica and copper slag using regression analysis and artificial neural networks. *Construction and Building Materials*. https://doi.org/10.1016/j.conbuildmat.2016.03.214

Cho, B. S., Kim, Y. U., Kim, D. B., & Choi, S. J. (2018). Effect of ferronickel slag powder on microhydration heat, flow, compressive strength, and drying shrinkage of mortar. *Advances in Civil Engineering*. https://doi.org/10.1155/2018/6420238

Choi, Y. C., & Choi, S. (2015). Alkali–silica reactivity of cementitious materials using ferro-nickel slag fine aggregates produced in different cooling conditions. *Construction and Building Materials, 99*, 279–287. https://doi.org/10.1016/j.conbuildmat.2015.09.039

Doğruyol, M. (2024). Determination of ASR in concrete using characterization methods. *Buildings*. https://doi.org/10.3390/buildings14030657

Dong, Q., Wang, G., Chen, X., Tan, J., & Gu, X. (2021). Recycling of steel slag aggregate in portland cement concrete: An overview. *Journal of Cleaner Production*. https://doi.org/10.1016/J.JCLEPRO.2020.124447

Fernandes, I., & Broekmans, M. A. T. M. (2013). Alkali-silica reactions: An overview. *Metallography, Microstructure, and Analysis, 2*(4), 257–267. https://doi.org/10.1007/S13632-013-0085-5/FIGURES/7

Figueira, R. B., Sousa, R., Coelho, L., Azenha, M., de Almeida, J. M., Jorge, P. A. S., & Silva, C. J. R. (2019). Alkali-silica reaction in concrete: Mechanisms, mitigation and test methods. *Construction and Building Materials, 222*, 903–931. https://doi.org/10.1016/J.CONBUILDMAT.2019.07.230

Flanders, W. D., Dersimonian, R., & Freedman, D. S. (1992). Interpretation of Linear Regression Models That Include Transformations or Interaction Terms.

Gao, J. (2024). R-Squared (R 2)-How much variation is explained? *Original Research Article Research Methods in Medicine & Health Sciences, 5*(4), 104–109. https://doi.org/10.1177/26320843231186398

Gholizadeh Vayghan, A., Rajabipour, F., & Rosenberger, J. L. (2016). Composition-rheology relationships in alkali-silica reaction gels and the impact on the gel's deleterious behavior. *Cement and Concrete Research, 83*, 45–56. https://doi.org/10.1016/J.CEMCONRES.2016.01.011

Glinicki, M. A., Bogusz, K., Jóźwiak-Niedźwiedzka, D., & Dąbrowski, M. (2023). ASR performance of concrete at external alkali supply-effects of aggregate mixtures and blended cement. *International Journal of Pavement Engineering*. https://doi.org/10.1080/10298436.2023.2171038

Guthrie, G. D., & Carey, J. W. (2015). A thermodynamic and kinetic model for paste-aggregate interactions and the alkali-silica reaction. *Cement and Concrete Research*. https://doi.org/10.1016/j.cemconres.2015.05.004

Haha, M. B., Gallucci, E., Guidoum, A., & Scrivener, K. L. (2007). Relation of expansion due to alkali silica reaction to the degree of reaction measured by SEM image analysis. *Cement and Concrete Research*. https://doi.org/10.1016/j.cemconres.2007.04.016

Han, F., Zhang, H., Li, Y., & Zhang, Z. (2023). Recycling and comprehensive utilization of ferronickel slag in concrete. *Journal of Cleaner Production, 414*, Article 137633. https://doi.org/10.1016/J.JCLEPRO.2023.137633

Huang, H., Shen, X., & Zheng, J. (2010). Modeling, analysis of interaction effects of several chemical additives on the strength development of silicate cement. *Construction and Building Materials*. https://doi.org/10.1016/j.conbuildmat.2010.04.007

Irmawaty, R., Caronge, M. A., Tjaronge, M. W., Abdurrahman, M. A., & Ahmad, S. B. (2023). Compressive strength and corrosion behavior of steel bars embedded in concrete produced with ferronickel slag aggregate and fly ash: An experimental study. *Innovative Infrastructure Solutions, 8*(7), 1–15. https://doi.org/10.1007/S41062-023-01162-1

Kim, K.-H., Oh, S.-R., Choi, W., & Choi, Y.-W. (2014). A study on the relationship between compressive strength and water-cement ratio according to water reducing ratio. *Journal of the Korea Concrete Institute, 26*(5), 591–598. https://doi.org/10.4334/JKCI.2014.26.5.591

Kumar Parhi, S., & Kumar Panigrahi, S. (2024). Alkali-silica reaction expansion prediction in concrete using hybrid metaheuristic optimized machine learning algorithms. *Asian Journal of Civil Engineering, 25*(3), 1091–1113. https://doi.org/10.1007/s42107-023-00799-8

Kurniati, E. O., Pederson, F., & Kim, H. J. (2023). Application of steel slags, ferronickel slags, and copper mining waste as construction materials: A review. *Resources, Conservation and Recycling, 198*, Article 107175. https://doi.org/10.1016/J.RESCONREC.2023.107175

Lei, J., Law, W. W., & Yang, E. H. (2021). Effect of calcium hydroxide on the alkali-silica reaction of alkali-activated slag mortars activated by sodium hydroxide. *Construction and Building Materials, 272*, Article 121868. https://doi.org/10.1016/J.CONBUILDMAT.2020.121868

Liu, X., Li, T., Tian, W., Wang, Y., & Chen, Y. (2020). Study on the durability of concrete with FNS fine aggregate. *Journal of Hazardous Materials*. https://doi.org/10.1016/j.jhazmat.2019.120936

Lokesha, E. B., Aruna, M., Reddy, S. K., & Srinivasa, A. S. (2023). Development of regression model and optimization of mechanical properties of geopolymer concrete prepared using gold ore tailings. *Journal of Hazardous, Toxic, and Radioactive Waste*. https://doi.org/10.1061/JHTRBP.HZENG-1259

Małek, M., Jackowski, M., Łasica, W., Dydek, K., & Boczkowska, A. (2021). An experimental study of possible post-war ferronickel slag waste disposal in Szklary (Lower Silesian, Poland) as partial aggregate substitute in concrete: Characterization of physical, mechanical, and thermal properties. *Materials*. https://doi.org/10.3390/MA14102552

Manso, J. M., Polanco, J. A., Losañez, M., & González, J. J. (2006). Durability of concrete made with EAF slag as aggregate. *Cement and Concrete Composites, 28*(6), 528–534. https://doi.org/10.1016/J.CEMCONCOMP.2006.02.008

Miura, T., Sato, K., Fujishima, M., Nakamura, H., & Kawabata, Y. (2022). Mechanism for reduction in compressive properties of cementitious materials in relation to internal crack patterns due to ASR and DEF expansion. *Cement and Concrete Composites, 128*, Article 104441. https://doi.org/10.1016/j.cemconcomp.2022.104441

Ngii, E., Kadir, A., Rachman, R. M., & Serah, M. (2021). Optimum combination of ferro-nickel slag (FeNi4) to the normal sand for the concrete compressive strength. *IOP Conference Series: Earth and Environmental Science, 622*(1), Article 012038. https://doi.org/10.1088/1755-1315/622/1/012038

Nguyen, Q. D., Castel, A., Kim, T., & Khan, M. S. H. (2021). Performance of fly ash concrete with ferronickel slag fine aggregate against alkali-silica reaction and chloride diffusion. *Cement and Concrete Research, 139*, Article 106265. https://doi.org/10.1016/j.cemconres.2020.106265

Nuruzzaman, M., Kuri, J. C., & Sarker, P. K. (2022). Strength, permeability and microstructure of self-compacting concrete with the dual use of ferronickel slag as fine aggregate and supplementary binder. *Construction and Building Materials*. https://doi.org/10.1016/j.conbuildmat.2021.125927

Olajide, O. D., Nokken, M. R., & Sanchez, L. F. M. (2023). Alkali-silica reactions: Literature review on the influence of moisture and temperature and the knowledge gap. *Materials, 17*(1), 10. https://doi.org/10.3390/MA17010010

Petrounias, P., Rogkala, A., Giannakopoulou, P. P., Christogerou, A., Lampropoulou, P., Liogris, S., et al. (2022). Utilization of industrial ferronickel slags as recycled concrete aggregates. *Applied Sciences, 12*(4), 2231. https://doi.org/10.3390/APP12042231

Popovics, S., & Ujhelyi, J. (2008). Contribution to the concrete strength versus water-cement ratio relationship. *Journal of Materials in Civil Engineering, 20*(7), 459–463. https://doi.org/10.1061/(ASCE)0899-1561(2008)20:7(459)/ASSET/1FD4AD97-FC8D-4777-8FCF-BEAF3F803A24/ASSETS/IMAGES/LARGE/5.JPG

Poyet, S., Sellier, A., Capra, B., Foray, G., Torrenti, J. M., Cognon, H., & Bourdarot, E. (2007). Chemical modelling of Alkali Silica reaction: Influence of the reactive aggregate size distribution. *Materials and Structures*. https://doi.org/10.1617/s11527-006-9139-3

Ruiz, E., & Freyne, S. (2020). Multiple regression model for load rating of reinforced concrete bridges. *Transportation Research Record, 2020*(7), 361–372. https://doi.org/10.1177/0361198120922546

Saha, A. K., & Sarker, P. K. (2016). Expansion due to alkali-silica reaction of ferronickel slag fine aggregate in OPC and blended cement mortars. *Construction and Building Materials, 123*, 135–142. https://doi.org/10.1016/j.conbuildmat.2016.06.144

Saha, A. K., & Sarker, P. K. (2017a). Sustainable use of ferronickel slag fine aggregate and fly ash in structural concrete: Mechanical properties and leaching study. *Journal of Cleaner Production, 162*, 438–448. https://doi.org/10.1016/J.JCLEPRO.2017.06.035

Saha, A. K., & Sarker, P. K. (2017b). Compressive strength of mortar containing ferronickel slag as replacement of natural sand. *Procedia Engineering, 171*, 689–694. https://doi.org/10.1016/j.proeng.2017.01.410

Saha, A. K., & Sarker, P. K. (2018). Durability of mortar incorporating ferronickel slag aggregate and supplementary cementitious materials subjected to wet-dry cycles. *International Journal of Concrete Structures and Materials, 12*(1), 1–12. https://doi.org/10.1186/S40069-018-0264-5

Saha, A. K., & Sarker, P. K. (2020). Effect of sulphate exposure on mortar consisting of ferronickel slag aggregate and supplementary cementitious materials. *Journal of Building Engineering*. https://doi.org/10.1016/j.jobe.2019.101012

Saha, A. K., Khan, M. N. N., & Sarker, P. K. (2018). Value added utilization of by-product electric furnace ferronickel slag as construction materials: A review. *Resources, Conservation and Recycling, 134*, 10–24. https://doi.org/10.1016/J.RESCONREC.2018.02.034

Saha, A. K., Sarker, P. K., & Majhi, S. (2019). Effect of elevated temperatures on concrete incorporating ferronickel slag as fine aggregate. *Fire and Materials, 43*(1), 8–21. https://doi.org/10.1002/FAM.2664

Shi, C., & Qian, J. (2000). High performance cementing materials from industrial slags - A review. *Resources, Conservation and Recycling, 29*(3), 195–207. https://doi.org/10.1016/S0921-3449(99)00060-9

Shi, Z., Shi, C., Zhao, R., & Wan, S. (2015). Comparison of alkali–silica reactions in alkali-activated slag and Portland cement mortars. *Materials and Structures/materiaux Et Constructions, 48*(3), 743–751. https://doi.org/10.1617/S11527-015-0535-4

Singh, S. B., Munjal, P., & Thammishetti, N. (2015). Role of water/cement ratio on strength development of cement mortar. *Journal of Building Engineering, 4*, 94–100. https://doi.org/10.1016/J.JOBE.2015.09.003

Sun, J., Feng, J., & Chen, Z. (2019). Effect of ferronickel slag as fine aggregate on properties of concrete. *Construction and Building Materials, 206*, 201–209. https://doi.org/10.1016/J.CONBUILDMAT.2019.01.187

Sun, J., Wang, Y., Yao, X., Ren, Z., Zhang, G., Zhang, C., et al. (2021). Machine-learning-aided prediction of flexural strength and ASR expansion for waste glass cementitious composite. *Applied Sciences*. https://doi.org/10.3390/app11156686

Sun, J., Wang, Z., & Chen, Z. (2018). Hydration mechanism of composite binders containing blast furnace ferronickel slag at different curing temperatures. *Journal of Thermal Analysis and Calorimetry, 131*(3), 2291–2301. https://doi.org/10.1007/S10973-017-6739-9/FIGURES/13

Tam, V. W. Y., Butera, A., Le, K. N., Da Silva, L. C. F., & Evangelista, A. C. J. (2022). A prediction model for compressive strength of CO 2 concrete using regression analysis and artificial neural networks. *Construction and Building Materials*. https://doi.org/10.1016/j.conbuildmat.2022.126689

Tang, H., Peng, Z., Shang, W., Ye, L., Luo, J., Rao, M., & Li, G. (2022). Preparation of refractory materials from electric furnace ferronickel slag and blast furnace ferronickel slag: A comparison. *Journal of Environmental Chemical Engineering*. https://doi.org/10.1016/j.jece.2022.107929

Tangahu, B. V., Warmadewanthi, I., Saptarini, D., Pudjiastuti, L., Tardan, M. A. M., Luqman, A., et al. (2015). Ferronickel slag performance from reclamation Area in Pomalaa, Southeast Sulawesi, Indonesia. *Advances in Chemical Engineering and Science, 5*(3), 408–412. https://doi.org/10.4236/ACES.2015.53041

Togawa, K., Shoya, M., & Kokubu, K. (1996). Characteristics of bleeding, freeze-thaw resistance and watertightness of concrete with ferro-nickel slag fine aggregates. *Zairyo/journal of the Society of Materials Science, Japan, 45*(1), 101–109. https://doi.org/10.2472/jsms.45.101

Wang, T., Nicolas, S., Nguyen, T. N., Kashani, A., & Ngo, T. (2023). Experimental and numerical study of long-term alkali-silica reaction (ASR) expansion in mortar with recycled glass. *Cement and Concrete Composites, 139*, Article 105043. https://doi.org/10.1016/j.cemconcomp.2023.105043

Wu, Y., Yang, J., Liu, X., Lu, Y., & Lu, R. (2024). Combined correlation analysis and multilinear regression for strength model of cement-stabilized clayey soils. *International Journal of Geomechanics*. https://doi.org/10.1061/IJGNAI.GMENG-9579

Xie, H. S., Gandla, S. R., Shi, O., & Solanki, P. (2023). Multivariate regression and variance in concrete curing methods: Strength prediction with experiments. *Applied Sciences*. https://doi.org/10.3390/app132212239

Yang, L., Lai, B., Xu, R., Hu, X., Su, H., Cusatis, G., & Shi, C. (2023). Prediction of alkali-silica reaction expansion of concrete using artificial neural networks. *Cement and Concrete Composites, 140*, Article 105073. https://doi.org/10.1016/j.cemconcomp.2023.105073

Yang, T., Zhang, Z., Wang, Q., & Wu, Q. (2020). ASR potential of nickel slag fine aggregate in blast furnace slag-fly ash geopolymer and Portland cement mortars. *Construction and Building Materials*. https://doi.org/10.1016/j.conbuildmat.2020.119990

Yiğiter, H., Yazici, H., & Aydin, S. (2007). Effects of cement type, water/cement ratio and cement content on sea water resistance of concrete. *Building and Environment, 42*(4), 1770–1776. https://doi.org/10.1016/J.BUILDENV.2006.01.008

Yu, Y., Nguyen, T. N., Li, J., Sanchez, L. F. M., & Nguyen, A. (2020). Predicting elastic modulus degradation of alkali silica reaction affected concrete using soft computing techniques: a comparative study. *Construction and Building Materials*. https://doi.org/10.1016/j.conbuildmat.2020.122024

Yu, Y., Zhang, C., Gu, X., & Cui, Y. (2019). Expansion prediction of alkali aggregate reactivity-affected concrete structures using a hybrid soft computing method. *Neural Computing and Applications*. https://doi.org/10.1007/s00521-018-3679-7

Zhang, J., Zhang, Y., Marani, A., & Zhang, L. (2024). A new understanding of the alkali-silica reaction expansion in concrete using a hybrid ensemble model. *Journal of Building Engineering*. https://doi.org/10.1016/j.jobe.2024.110523

Publisher's Note

Tae Yeon Kim Graduate student, Department of Smart City Engineering, Hanyang University, Sangnok-gu, Ansan-si, Republic of Korea, 15,588.

Sun Gyu Park Professor, Department of Architectural Engineering, Mokwon University, Seo-gu, Daejeon, Republic of Korea, 35,349.

Woo Jin Lee Department Head, Engineering Center, Samsung C&T, Gangdong-gu, Seoul, Republic of Korea, 05288.

Jae Hun Jung Graduate student, Department of Smart City Engineering, Hanyang University, Sangnok-gu, Ansan-si, Republic of Korea, 15,588.

Jun Chul Yoon Graduate student, Department of Smart City Engineering, Hanyang University, Sangnok-gu, Ansan-si, Republic of Korea, 15,588.

Kadepalli Nagendra Shivaprasad Research Assistant Professor, Centre for AI Technology in Construction, Hanyang University, Sangnok-gu, Ansan-si, South Korea, 15,588.

Hyun Min Yang Assistant Professor, Division of Smart Convergence Engineering, Hanyang University, Sangnok-gu, Ansan-si South Korea, 15,588.